Strategies towards thermochemical valorisation of spent coffee grounds (SCG): kinetic analysis of the thermal and thermo-oxidative decomposition

C. Primaz, O. Gil-Castell*, A. Ribes-Greus*

DOI:

https://doi.org/10.1016/j.biombioe.2023.106840

Please, cite it as:

C. Primaz, O. Gil-Castell, A. Ribes-Greus. Strategies towards thermochemical valorisation of spent coffee grounds (SCG): kinetic analysis of the thermal and thermo-oxidative decomposition. Biomass and Bioenergy 2023:174;106840

Instituto de Tecnología de Materiales (ITM). Universitat Politècnica de València. Camino de Vera s/n, 46022 Valencia, Spain.

*Corresponding author:

O. Gil-Castell ogilcastell@doctor.upv.es, A. Ribes-Greus aribes@ter.upv.es

Strategies towards thermochemical valorisation of spent coffee grounds (SCG): kinetic analysis of the thermal and thermo-oxidative decomposition

C. Primaz, O. Gil-Castell*, A. Ribes-Greus*

Instituto de Tecnología de Materiales (ITM), Universitat Politècnica de València (UPV). Camino de Vera s/n, 46022 Valencia, Spain.

*Corresponding authors: ogilcastell@doctor.upv.es, aribes@ter.upv.es

Abstract

The thermochemical conversion of spent coffee grounds (SCG) under inert and oxidative conditions was comprehensively evaluated as a feasible valorisation route for this biomass. Dynamic thermogravimetric assays were carried out at different heating rates, where the individual contribution of the pseudo-components (hemicellulose, cellulose, lignin) was assessed by a deconvolution approach with Lorentz curves. The kinetic triplet, constituted by the apparent activation energy (E_a), the pre-exponential factor (A) and the model of reaction ($g(a)$), was defined for each pseudo-component through the application of iso-conversional methods, Master-Curves and Perez-Maqueda criterion. Under an inert atmosphere, the devolatilisation of humidity, decomposition of hemicellulose, cellulose and part of lignin, and finally the completion of lignin were identified, resulting in a remaining percentage of 20% of biochar. For hemicellulose, E_a was 217 kJ·mol^{-1}, for cellulose 214 kJ·mol^{-1}, and lignin 151 kJ·mol^{-1}. Under oxidative conditions, analogous mass-loss stages were found, with the only difference being that biochar was decomposed until only ash (~2%) was obtained as residue. The advantage of using SCG as biofuels, with a high LHV and HHV (~20 MJ·kg^{-1}), was thus demonstrated. The E_a for the hemicellulose was 194 kJ·mol^{-1}, for cellulose 147 kJ·mol^{-1}, and for lignin was 173 kJ·mol^{-1}. Similar decomposition paths were found regardless of the atmosphere for hemicellulose (F_4), hemicellulose (D_3), and lignin ($F_{2/4}$), which suggests that the temperature, the reactant concentration, the particle shape and the diffusion of products control the decomposition of SCG during non-isothermal pyrolytic or combustive thermochemical processes.

Keywords

Biomass, spent coffee ground, kinetic analysis, pyrolysis, combustion

1. Introduction

The use of renewable products in the energy field can offer alternatives to fossil fuels to meet the growing energy demand from a sustainable perspective. The energy valorisation of biomass is a promising alternative, although it requires an in-depth evaluation of feedstocks, pre-treatment or fractionation [1]. Biomass is the oldest renewable energy source for humans and covers an essential role in the strategic push for sustainable development [2,3]. Lignocellulosic biomass (LCB), with a global annual production of 181.5 billion tonnes [4], is a natural, directly available, cheap and renewable feedstock composed of cellulose, hemicellulose and lignin, with variable relative percentages depending on the type, species, and origin of the biomass [5].

Biomass can come from forest residues and industrial or agri-food by-products. This is the case of the spent coffee grounds (SCG), which are the primary wastes from the coffee industries. In numbers, 1 ton of green coffee generates about 650 kg of SCG during coffee drink production [6]. In addition, for the production of soluble coffee, about 2 kg of wet SCG are obtained for every 1 kg of soluble coffee produced [7,8]. This represents a worldwide annual production of SCG of close to 6 million tons. SCG are characterised by fine particle size, humidity, organic load and acidity [9]. Such acidity particularly results from the preparation of soluble coffee, where raw coffee powder is treated with hot water or steam. Although the disposal of SCG at landfills is discouraged, it is still practised in most developing countries worldwide. Apart from landfilling costs, the leachate generated by SCG can deteriorate the soil and groundwater. Besides, SCG contain many recalcitrant compounds, such as caffeine, tannins, and polyphenols, together with the production of methane during its decomposition [10,11], which encourages searching for alternatives to landfill. In this regard, the reuse of SCG is becoming an expanding field, converting them into value-added products convenient from an environmental and economic perspective [12].

The circular economy principle involves that industrial wastes may be reused as raw materials for new processes while guaranteeing the overall reduction of waste, generating economic benefits, and decreasing the environmental impact [13]. Applied to SCG, they can be materially valorised as a source

of biochemical nutrients, antioxidants or polysaccharides with immunostimulatory activity, soil amendment in agriculture, heavy metal or CO_2 absorbent, or filler to prepare biocomposites, among others [14–20]. Even though the high lignin content may prevent its direct application in food, the improvement of extraction methods allowed for obtaining bioactive compounds for the pharmaceutical industry [21]. SCG have also been explored from an energetic perspective to get biodiesel, bioethanol, bio-ethers, bio-oil, biochar, and biogas [22–27], also considering anaerobic digestion strategies [28]. Finally, the thermochemical conversion of SCG stands as a promising route for obtaining gas, liquid or solid biofuels and bioenergy. Pyrolysis and combustion are considered among the best processes for the thermochemical conversion of SCG, both as pure feedstock [29–38] or in combination with other organic residues [39–43].

In environments with a total absence of oxygen, except for cases where partial combustion may supply the thermal energy necessary for the process, the non-exothermic decomposition pyrolytic process involves biomass's thermal conversion into gas, liquid, and solid at temperatures above 300–400 °C [44–46]. Thermal decomposition reactions involve chain breakages, molecular weight reduction, and recombinations of chemical bonds to form new compounds used as biofuels or chemical inputs. From this reaction, by-products involve (*i*) pyrolytic gas (volatile matter) composed mainly of carbon monoxide (CO), carbon dioxide (CO_2), hydrogen (H_2), light hydrocarbons, traces of other organic components, and water vapour; (*ii*) bio-oil, a dark-coloured liquid, which originates from condensable organic vapours; and (*iii*) biochar, a solid rich in carbon. The yield and properties of these products depend on the nature of the raw material, the type of reactor, and the operating conditions (temperature, heating rate, or vapour residence time). The thermal decomposition process of SCG has been recently kinetically studied by Brachi *et al.* with a strategy for evaluating global decomposition in an inert atmosphere [31]. Kelkar *et al*. also encouraged using SCG in pyrolysis pilot-scale as a waste-to-energy opportunity and obtained high bio-oil yield enriched in higher-value fatty acids [33,47]. Complementarily, Pil Bok *et al.* assessed the fast pyrolysis of coffee grounds and studied the characteristics of product yields and biocrude oil quality [48]. In this line, Tsai *et al.* also assessed the

fuel properties of biochar from the pyrolysis of exhausted coffee residue [49]. Finally, Fu *et al.* recently assessed the effects of a previous torrefaction procedure on the pyrolytic performance of SCG [32].

Differently, when the fuel reacts with an oxidant, air or pure oxygen, an exothermic chemical combustive reaction occurs, accompanied by heat production and chemical species conversion. In an entirely oxidative reaction, fuel reacts with the oxidising element, and the products are oxidised compounds of each pseudo-component of a given fuel. Competitive reactions occur ascribed to oxidative and/or thermal sub-processes during the global course. Heat and electricity are two principal forms of energy derived from biomass thermo-oxidation. While industrial heating is produced by steam generated in biomass-fired boilers, producing electricity usually involves biomass combustion and a steam turbine. Therefore, this thermochemical process pursues converting chemical energy contained in the fuel into sensible heat [1,50,51]. According to the International Coffee Organization (ICO), SCG can be used in boilers as a combustible material thanks to their high calorific value and direct energy source [52]. Fresh SCG include water content between 55 and 80% so that for converting them into an energy source, moisture content must be below 12.5% [53]. This ensures safe storage, reduces transportation weight, removes odours and reduces the possibility of microorganism growth [54]. In this line, Tun *et al.* deeply evaluated the drying process of SCG for being used as a renewable energy source [54]. Complementarily, Ciesielczuk *et al.* explored the possibility of converting SCG into briquettes and using them as a source of energy in combustion processes [55]. Limousy *et al*. studied the gaseous products and particulate matter emissions of residential biomass boiler fired with pellets of SCG [36,37]. Other studies testing the combustion of SCG [35,38,42] and mixed pellets of SCG and sawdust [41] in pilot-scale boiler plants may also be mentioned.

For both pyrolytic and combustive processes, understanding the progression of decomposition-reaction and the dependence of the rate on process parameters is crucial, and can be achieved by conducting a kinetic study from thermogravimetric analysis data [56–58]. The knowledge of kinetic parameters such as activation energy, pre-exponential factor, and reaction model is vital in designing and optimizing pyrolysis or combustion reactors, predicting material lifetime, CFD modelling, and establishing process

conditions. For complex biomass mixtures, where the nature of the reaction changes during progression, isoconversional methods are ideally suited to determine activation energy, which assume that at a constant activation energy value, the rate of reaction is a function of temperature only [59,60]. Isoconversional methods consist of several differential and integral methods, including the Friedman method [61], Flynn-Wall-Ozawa (FWO) method [62], Kissinger-Akahira-Sunose (KAS) equation [63], and others [64–67].

Even though some of the previously referenced studies explored the use of SCG in thermochemical conversion processes under inert or oxidative environments in pyrolytic or combustive processes, respectively, there is a lack of studies in the literature dealing with a comprehensive comparative evaluation of the particular decomposition courses of the different pseudo-components in the SCG. Considering biomass decomposition as a one-step reaction is unsuitable, especially when the apparent activation energy varies with conversion, representing a complex performance involving mechanism changes which are hard to be determined [68]. Therefore, this study pursues the novel aim to fill the knowledge gap of assessing the individual and separate kinetic performance of the main constituents of SCG, i.e. hemicellulose, cellulose and lignin, under simulated pyrolytic and combustive environments using thermogravimetric analysis (TGA). For this purpose, the particular objectives of this study are to (1) evaluate thermal and thermo-oxidative decomposition of SCG during dynamic experiments involving non-isothermal multiple heating, (2) deconvolute the DTG curves using Lorentz curves for separating the contribution of hemicellulose, cellulose and lignin, (3) approximate the activation energy, the kinetic function and the pre-exponential factor through a systematic and comparative strategy for determining the kinetic parameters for SCG. These analyses define the kinetic models of such reactions, which are essential knowledge for optimising the design of pyrolysis or combustion process reactors that allow for appropriate thermochemical conversion.

2. Materials and methods

2.1. Spent coffee grounds (SCG)

The analysed spent coffee grounds (SCG) were the residue generated after the preparation of the coffee drink by filtering the coffee powder with hot water at ~80 °C. The SCG were left for water draining at ~20 °C overnight and subsequently dried in a Heraeus LUT6050 convection oven at 105 °C for 2 h to remove moisture [54]. The microscopic structure of the studied SCG, with a heterogeneous morphology and a maximum particle size of 250 μm (sieved through a 60 mesh), is shown in **Figure S1** of the Supplementary Material.

2.2. Proximate and ultimate analyses

Ash (*A*), volatile matter (*VM*), and moisture (*M*) contents of the SCG were measured according to the standardised procedures described in ISO 18122:2016 (Solid Biofuels – Determination of ash content) [69], ISO 18123:2016 (Solid biofuels – Determination of the content of volatile matter) [70], and ISO 18134-1:2016 (Solid biofuels – Determination of moisture content – Oven dry method – Part 1: Total moisture – Reference method) [71], respectively. The fixed carbon (*FC*) was determined by the difference between these values, according to **Equation 1**. Moisture content was determined after drying in a Heraeus Vacutherm oven, while volatile matter and ashes were determined with the aid of a Thermo Heraeus M-104 muffle furnace, all of them carried out in triplicates.

$$FC(\%) = 100 - M\ (\%) - VM\ (\%) - A\ (\%) \qquad (\mathbf{1})$$

The ultimate analysis of SCG in terms of Carbon (C), Hydrogen (H), Nitrogen (N), Sulphur (S), and Oxygen (O) was determined using a CHNS-O Thermo Flash 2000 elemental analyser, operating at 900 °C in an atmosphere of pure oxygen. The oxygen content was calculated by the difference on a dry and ash-free basis according to **Equation 2**.

$$O(\%) = 100 - C(\%) - H(\%) - N(\%) - S(\%) \qquad (\mathbf{2})$$

2.3. Thermogravimetric analysis (TGA)

Thermogravimetric analysis (TGA) was conducted to characterise the biomass's thermal and thermo-oxidative decomposition process under simulated pyrolytic and combustion conditions. The analyses were performed on a Mettler Toledo TGA/SDTA 851 module. Samples of approximately 7 mg were heated on alumina crucibles with a capacity of 70 μL. The experiments were performed in the temperature range from 25 °C to 800 °C at a heating rate of 2, 5, 10, 15 and 20 °C·min^{-1}, under inert and oxidative atmospheres of argon and oxygen, respectively, at a gas flow rate of 50 mL·min^{-1}. The obtained results were evaluated using the STARe 9.10 software. At least three specimens per sample were analysed, and the averages were considered representative.

2.3.1. Deconvolution: multiple peak fitting

During thermogravimetric analysis, pseudo-components' decomposition and subsequent degradation by-products can occur. These processes can be grouped into (*i*) volatilisation and (*ii*) char-forming reactions. Even though these processes can occur separately for each component of a given material, they usually coincide, provoking overlapping and preventing the separated study of each component. In this regard, deconvolution allows separating the whole curve into several sub-processes correlated to the decomposition of different pseudo-components. This strategy is usually applied in the first derivative thermogravimetric curve (DTG) and assumes that the experimental curve is the sum of the individual curves, in which the reactivity of the decomposition regions is proportional to the height of the DTG peak [72]. Moreover, this analysis accepts that the decomposition of each component happens in a single stage, according to the reported temperature ranges for the degradation of hemicellulose, cellulose, and lignin. These assumptions do not produce significant deviations from the reality of the thermal decomposition of lignocellulosic biomass [73].

The model curves are meant to reproduce the experimental DTG curve by minimising the differences between their ordinates through a criterion such as least-squares [74]. The most common among the theoretical functions are the symmetric Gaussian, Lorentz, Laplace, and Pearson VII, and the asymmetric Suzuki-Fraser or Asymmetric Double Sigmoidal functions [75–80]. Although the use of

asymmetric functions may be more representative of reality, in this work the authors found difficulties in obtaining reliable results that were kinetically consistent at the different heating rates when applying asymmetric functions. The close confluence and simultaneous overlapping of the decomposition processes of the pseudo-components in the thermogravimetric made it a challenging task to set the appropriate shape analysis of the kinetic curves, and therefore to separate their contribution to the overall curve. Therefore, after a prior testing and optimization process, this study proposes deconvolution using the multi-peak Lorentz fitting method, showing the best fitting results. According to previous reports in the literature for the composition of spent coffee grounds [10,81,82] and its thermal decomposition [23,24,48], the overlapping peaks were separated into five sub-peaks, corresponding to water, hemicellulose, cellulose, lignin, and char. The fitting was performed, therefore, by optimisation of three parameters: centre (x_c); amplitude (A); and width at half of the maximum height (ω), according to **Equation 3**.

$$y = y_0 + \frac{2A}{\pi} \cdot \frac{\omega}{4(x-xc)^2+\omega^2} \quad (3)$$

where x is the independent variable, and y_0 is the initial value of the Lorentz function at x_0.

2.4. Kinetic analysis of the thermal and thermo-oxidative decomposition of biomass

Kinetic analysis is characterised by the definition of kinetic triplet, involving the activation energy (E_a), the pre-exponential factor (A), and the kinetic function ($f(\alpha)$) of a given process. The thermal decomposition rate involves the contribution of the reactant concentration and the reaction rate (k), depending on the absolute temperature. The Arrhenius equation describes the reaction rate (k), while the reactant concentration in the thermal decomposition process is represented in terms of mass loss at every time (ω). This reactant concentration can also be defined by the conversion degree (α), equal to the ratio between the sample mass lost at a time t and the sample mass lost at an infinite time or total mass loss. The Arrhenius equation, the kinetic equation, the decomposition degree, and the rate equation are all reported in **Table 1**, where R is the universal gas constant; T is the absolute temperature; E_a is the

activation energy; *A* is the pre-exponential factor, assumed independent of temperature; ω is the actual mass of the sample (at time *t*); ω_0 is the initial mass of the sample; and ω_∞ is final mass of the sample.

Table 1. Equations applied to determine the final rate equation.

Arrhenius equation	
$k(T) = A \cdot e^{\left(-\frac{E_a}{RT}\right)}$	**(4)**
Kinetic equation	
$\frac{d\omega}{dt} = -\omega \cdot A \cdot e^{\left(\frac{E_a}{RT}\right)}$	**(5)**
Decomposition degree (α)	
$\alpha = \frac{\omega_0 - \omega}{\omega_0 - \omega_\infty}$	**(6)**
Rate equation	
$\frac{da}{dt} = f(a) \cdot A \cdot e^{\left(-\frac{E_a}{RT}\right)}$	**(7)**

2.4.1. Calculation of the apparent activation energy

The activation energy (E_a) can be calculated by adopting differential and integral models based on the analysis at multiple heating rates, assuming the given kinetic function and mathematical treatment of the general kinetic law. Differential and integral approaches were applied in this study to determine the activation energy, using data from different multi-linear dynamic experiments and avoiding model assumptions for the analysis. These strategies approximate the value of the activation energy for a given α and are called iso-conversional methods. In this work, integral methods proposed by Flynn-Wall-Ozawa (FWO) and Kissinger-Akahira-Sunose (KAS) were considered, while the differential method given by Friedman was applied, all of them shown in **Table 2** [62,63,83].

Table 2. Integral and differential expressions used for the calculation of the activation energy.

Integral methods	**Flynn-Wall-Ozawa (FWO)**	
	$\log\beta = \log\frac{Ea \cdot A}{R \cdot g(\alpha)} - 2.315 - \frac{0.457 \cdot Ea}{R \cdot T}$	(**8**)
	Kissinger-Akahira-Sunose (KAS)	
	$\ln\left(\frac{\beta}{T^2}\right) = \ln\left(\frac{A \cdot R}{Ea \cdot g(\alpha)}\right) - \frac{Ea}{R} \cdot \frac{1}{T}$	(**9**)
Differential method	**Friedman**	
	$\ln\left(\frac{d\alpha}{dt}\right) = \ln(A \cdot f(\alpha)) - \frac{Ea}{R} \cdot \frac{1}{T}$	(**10**)

2.4.2. Analysis of kinetic function

Master-Plots (*MP*) were used to estimate the kinetic function. This method uses theoretical curves independent of the kinetic parameters of the process but depends on the kinetic model. Obtaining appropriate kinetic models requires transforming the TGA data into experimental curves (MP_e) and comparing them with the theoretical *MP*. Although there are theoretical reference curves based on the differential form (MP_f) and the integral form (MP_g), the combination of both differential and integral forms (MP_{fg}) of the generalised kinetic equation was considered. As described by Criado, these curves are usually reduced considering the factor α=0.5 to obtain a better visualisation [84]. Then, the kinetic analysis can be carried out with a single-step kinetic equation, considering the activation energy found using the iso-conventional methods previously described. The inverse integral kinetic function *g(α)* can be obtained by developing the integral of the rate equation, as shown in **Equation 11**.

$$g(\alpha) = \int_0^{\alpha} \frac{d\alpha}{f(\alpha)} = \frac{A \cdot E_a}{\beta \cdot R} \cdot \int_0^{\infty} \frac{e^{-x}}{x^2} = \frac{A \cdot E_a}{R \cdot T} \cdot p(x) \qquad (\mathbf{11})$$

where $x = \frac{E_a}{RT}$; and $p(x) = \frac{e^{-x}}{x^2} * \sum_n \frac{n*(1-n)}{x+2*(n+1)}$ is the Senum and Yang approximation, which was truncated in the fifth term, leading to a good approximation for the exact temperature integral for x>10 [85]. By plotting the experimental curves (MP_e) at different α, it is possible to graphically compare and correlate with the theoretical master curves.

To determine the rate equation, it is essential to underline that *f(α)* depends on the degradation reaction pathway. In this regard, **Table 3** provides some examples of the most commonly used differential *f(α)* and integral *g(α)* functions for thermal and thermo-oxidative decomposition models of a full-scale system [86]. In these equations, mass and heat transfer limitations are absent since they result from a simplified reaction pathway, in which only the behaviour of the reaction in terms of intrinsic kinetics is considered, and not the whole complex network of reactions that characterises each reaction phase.

Table 3. Algebraic expressions for the most applied differential *f(α)* and integral *g(α)* functions of solid-state processes.

Symbol	f(α)	g(α)	Solid-state processes
		Sigmoidal curves	
A_2	$2(1-\alpha)[-\ln(1-\alpha)]^{-1}$	$[-\ln(1-\alpha)]^{\frac{1}{2}}$	Nucleation and growth (Avrami equation 1)
A_3	$3(1-\alpha)[-\ln(1-\alpha)]^{-1}$	$[-\ln(1-\alpha)]^{\frac{1}{3}}$	Nucleation and growth (Avrami equation 2)
A_4	$4(1-\alpha)[-\ln(1-\alpha)]^{-1}$	$[-\ln(1-\alpha)]^{\frac{1}{4}}$	Nucleation and growth (Avrami equation 3)
		Deceleration curves	
R_1	1	α	Phase boundary controlled reaction (one-dimensional movement)
R_2	$2(1-\alpha)^{\frac{1}{2}}$	$\left[1-\ln(1-\alpha)^{\frac{1}{2}}\right]$	Phase boundary controlled reaction (contracting area)
R_3	$3(1-\alpha)^{\frac{2}{3}}$	$\left[1-ln(1-\alpha)^{\frac{1}{3}}\right]$	Phase boundary controlled reaction (contracting volume)
D_1	$\frac{1}{(2a)}$	α^2	One-dimensional diffusion
D_2	$\frac{-1}{\ln(1-a)}$	$(1-\alpha)\ln(1-\alpha)+\alpha$	Two-dimensional diffusion
D_3	$\frac{3(1-a)^{\frac{2}{3}}}{2[1-(1-a)^{\frac{1}{3}}]}$	$\left[1-(1-\alpha)^{\frac{1}{3}}\right]^2$	Three-dimensional diffusion
D_4	$\frac{3}{2}[(1-a)^{\frac{1}{3}}-1]$	$\left[1-\frac{2}{3}a\right]-(1-a)^{\frac{2}{3}}$	Three-dimensional diffusion
F_1	$1-\alpha$	$-\ln(1-\alpha)$	Random nucleation with one nucleus on the individual particle
F_2	$(1-\alpha)^2$	$\frac{1}{(1-\alpha)}$	Random nucleation with two nuclei on the individual particle
F_3	$\frac{1}{2}(1-\alpha)^3$	$\frac{1}{(1-\alpha)^2}$	Random nucleation with three nuclei on the individual particle

2.4.3. Analysis of pre-exponential factor

The last step for the kinetic analysis involves determining the pre-exponential factor (*A*). For this purpose, the Perez-Maqueda criterion (*P-Mc*) must be satisfied [87]. This includes the independence of the activation parameters E_a and *A* with respect to the heating rate (β) and must be assessed with the Coats-Redfern expression shown in **Equation 12** [88].

$$\ln\frac{\beta \cdot g(\alpha)}{T^2} = \ln\frac{A \cdot R}{Ea} + \frac{E_a}{R} \cdot \frac{1}{T} \qquad (\mathbf{12})$$

Once calculated the activation energy from iso-conversional methods and known the reaction model using master plots, the best *n* order of the kinetic model was established by minimising **Equation 13**.

$$\xi(n,\alpha) = \sum_i^h \left| (-R) \cdot \frac{d}{dt}\left(\frac{\ln(\beta_i \cdot T^{-2} \cdot g(\alpha))}{T^{-1}}\right) - E_{a_{iso}} \right| \qquad (\mathbf{13})$$

The points with the best *n* must be on the same straight line for all heating rates. The pre-exponential factor (*A*) is consequently the average of the values A_β from the intercept at *y=0* of the Coats-Redfern equation.

3. Results and discussion

3.1. SCG biomass characterisation

Table 4 presents the proximate analysis, ultimate analysis, and calorific value of SCG. It was demonstrated that the applied drying procedure at 105 °C for 2 h reduced moisture to nearly 11% for using SCG as an energy source, as recently proven by Tun *et al.* [54]. The high volatile matter content can be highlighted, with a percentage close to 95% and a low ash yield of nearly 2%. The ultimate analysis reveals a high carbon and oxygen content, which confirms the lignocellulosic nature of SCG. The high percentage of carbon (~50%) also implies high calorific values (HHV and LHV close to 20 $MJ \cdot kg^{-1}$), which points out the convenience of using this biomass as a sustainable source for energy production in thermochemical conversion processes. It should also be noticed that the nitrogen's low content (<3%) reduces the possibilities of production of NO_x compounds during combustion, which, together with all the mentioned results, encourages the use of this material for bioenergy production. All

these results align with what has been reported in other studies dealing with powder and pellets of SCG [19,25,32,33,37–40,44,48,49,89].

Table 4. Proximate analysis, ultimate analysis and calorific value of SCG [44].

Proximate analysis	
Moisture (%)	11.37 ± 0.08
Ash yield (%)	2.24 ± 0.58
Volatile matter (%)	93.84 ± 0.58
Fixed Carbon (%)*	3.92 ± 1.06
Ultimate analysis	
N (%)	2.79 ± 0.08
C (%)	49.18 ± 0.05
H (%)	6.52 ± 0.29
O (%)	41.51 ± 0.42
H/C	0.13 ± 0.01
O/C	0.84 ± 0.01
Calorific value	
HHV ($MJ \cdot kg^{-1}$)	20.46 ± 0.11
LHV ($MJ \cdot kg^{-1}$)	19.25 ± 0.35

3.2. Thermal decomposition under inert conditions

The thermal stability of SCG under inert conditions was first assessed, and the obtained thermogravimetry (TG) and its first derivative (DTG) curves are shown in **Figure 1**. During heating, the TGA thermograms revealed a progressive decreasing trend during multiple mass-loss stages until a constant mass was reached. These mass loss regions can be correlated to the release of humidity followed by the depolymerisation and thermal decomposition of the pseudo-components of lignocellulosic biomass. Particularly for SCG, although degradation of several low-molar mass organic compounds, including proteins, fats or polysaccharides, can occur in the beginning, the stages of hemicellulose, cellulose and lignin degradation could be identified [23,24,48]. In detail, the initial mass reduction with a contribution of ~7% from 25 °C to 175 °C is related to free and bound moisture vaporisation [90,91]. This stage is followed by the decomposition of hemicellulose, occurring in the temperature range from 160 °C to 300 °C, with a mass loss of ~34%. The cellulose decomposition arises between 300 °C and 340 °C, with a mass loss of ~12%. Finally, the lignin decomposition appears between 340 °C and 420 °C with a ~13% mass loss. Indeed, in the range from 150 to 500 ºC,

dihydroxylation, demethoxylation, depolymerisation, fusion and degradation by breaking and releasing functional groups have been reported, revealing that the pyrolytic degradation of lignocellulosic biomass occurs through a set of complex reactions involving both physical and chemical inter and intra-particles phenomena [58]. The last decomposition, related to the char, is above 430 °C and continues slowly until 550 °C. At the end of the analysis, a blackish residue (*R*) with a mass percentage of ~20% may be ascribed to the remnant biochar containing fixed carbon and ash. All these stages are in line with previous reports for the pyrolysis of lignocellulosic biomass [40,56]

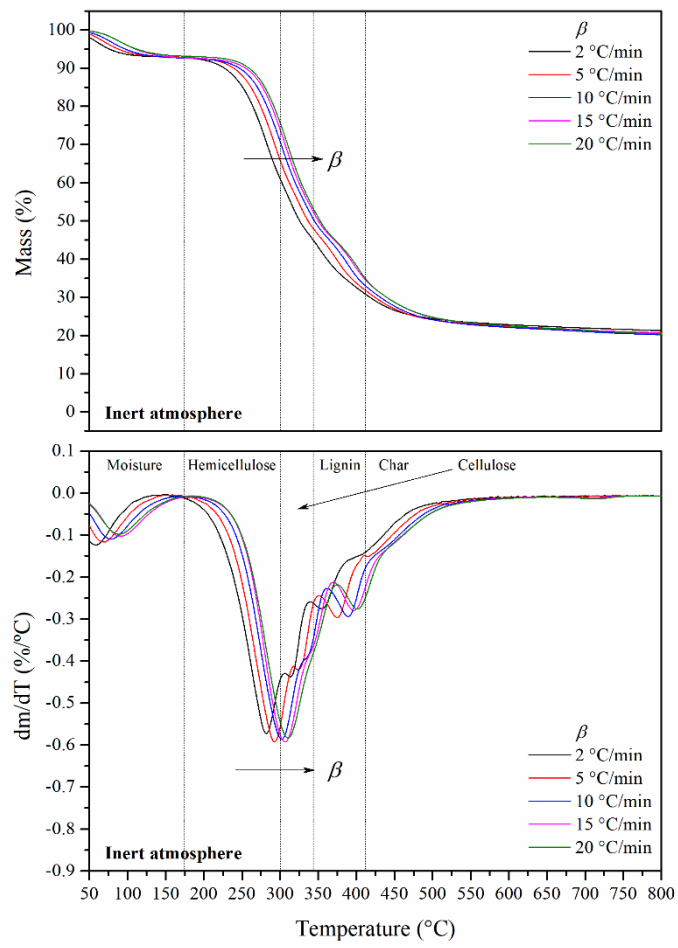

Figure 1. Thermogravimetric thermograms (TG) and their first derivative traces (DTG) of SCG under an inert atmosphere at β 2, 5, 10, 15, 20 °C·min^{-1}.

A detailed characterisation of the thermal decomposition process was considered, assessing the peak temperature (T_p) and the mass loss percentages (Δm) for the different processes, along with the onset

and endset degradation temperatures (T_o, T_e) for the principal mass loss stage. All these results are gathered in **Table 5**, and are in line with what has been reported in the literature for the pyrolytic decomposition of hemicellulose, cellulose and lignin in lignocellulosic biomass [76,92], spent coffee grounds [24,31,43] and other coffee-related biomass [50].

Table 5. Onset and endset degradation temperatures (T_o, T_e), residue (R) and peak temperature (T_p) and mass loss percentages for the different noticeable decomposition stages (Δm) obtained at β 2, 5, 10, 15 and 20 °C·min^{-1} under an inert atmosphere.

β (°C·min^{-1})	Water		Hemicellulose		Cellulose		Lignin		R (%)	T_o (°C)	T_e (°C)
	T_{po} (°C)	Δm_o (%)	T_{p1} (°C)	Δm_1 (%)	T_{p2} (°C)	Δm_2 (%)	T_{p3} (°C)	Δm_3 (%)			
2	57.0	6.6	280.1	34.7	311.9	11.2	349.6	10.1	22.2	245.9	478.7
5	70.1	7.0	292.4	35.5	323.8	9.8	374.1	11.3	23.1	256.5	482.6
10	80.4	7.5	301.8	34.5	334.3	12.1	386.3	13.6	20.5	264.9	508.9
15	90.4	7.3	306.4	32.4	-	14.6	395.7	13.5	20.9	269.9	512.3
20	88.9	6.8	310.7	33.6	-	14.5	401.4	13.5	20.7	272.8	521.7

In kinetic terms, when the heating rate increased, the decomposition ranges for all the stages were generally widened and moved towards higher temperatures. Nevertheless, the main thermal profile remained constant regardless of the heating rate, implying a similar degradation performance, as already found for the pyrolysis of SCG [31]. Faster heating limited heat transfer processes and, therefore, peak temperatures in the DTG curves increased [59,90,93]. Moreover, high heating rates reduce the time interval to which the sample is subjected at a given temperature, and consequently, less conversion occurs. Particularly for SCG, it was suggested that a lower heating rate allows for a higher yield of biochar, while higher rates enhance bio-oil production [31]. In terms of pseudo-components, their peak temperatures could be identified at low heating rates (2, 5, and 10 °C·min^{-1}). Nevertheless, higher heating rates (15 and 20 °C·min^{-1}) merged the peaks of cellulose and hemicellulose, as found in other studies dealing with the pyrolysis of lignocellulosic biomass [94]. For a graphical interpretation of the contribution of the heating rate, the onset and endset temperatures (T_o, T_e) and peaks for hemicellulose (T_{p1}), cellulose (T_{p2}), and lignin (T_{p3}) are plotted in **Figure 2** as a function of the heating rate. This representation shows that the zero-decomposition temperature (*ZDT*) can be calculated when the heating

rate tends to zero. This evaluation allows for predicting the thermal behaviour of a given biomass for a virtually null heating rate, avoiding the influence of the dynamic heating program. For this purpose, the exponential relationship shown in **Equation 14** may be considered, where *a*, *b* and *k* are the fitting parameters.

$$ZDT(\beta) = \frac{a}{1+b*e^{-k*\beta}} \quad \textbf{(14)}$$

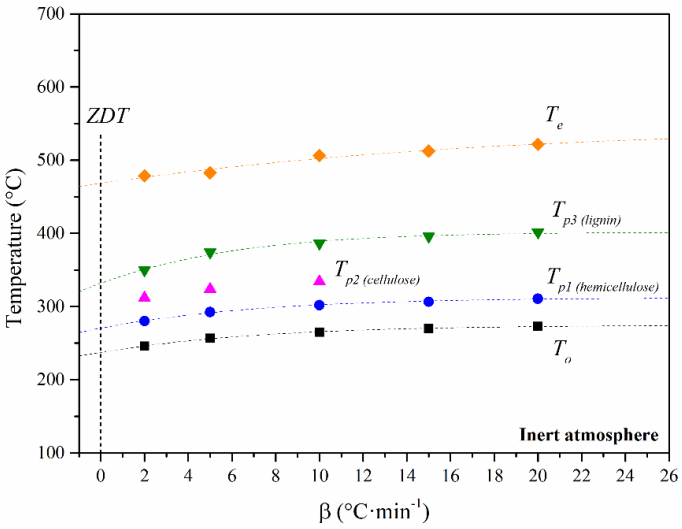

Figure 2. Evolution of the characteristic decomposition temperatures T_o, T_e, $T_{p1\ (hemicellulose)}$, $T_{p2\ (cellulose)}$, and $T_{p3\ (lignin)}$ at β of 2, 5, 10, 15, 20 °C·min^{-1} under an inert atmosphere.

The obtained *ZDT* values are reported in **Table 6** for all the studied parameters with regression coefficients above 0.97. Overall, when β tends to zero, the onset temperature for the thermal decomposition of SCG was 237 °C, the degradation of the hemicellulose starts at 271 °C, that of cellulose at 301 ºC, lignin at 332 °C and the endset of the pyrolytic process was estimated at 470 °C.

Table 6. *ZDT* values ($\beta \rightarrow 0$) along with the fitting parameters (*a*, *b* and *k*) and regression coefficients for the onset (T_o), endset (T_e), hemicellulose (T_{p1}), and lignin (T_{p3}) decomposition temperatures under an inert atmosphere.

	***ZDT* ($\beta \rightarrow 0$) (°C)**	***a***	***b***	***k***	R^2
Onset (T_o)	237.2	274.5	0.16	0.15	0.99
Hemicellulose (T_{p1})	271.5	311.9	0.15	0.16	0.99
Cellulose (T_{p2})	301.5	347.2	0.15	0.14	0.99
Lignin (T_{p3})	332.3	401.6	0.21	0.19	0.97
Endset (T_e)	470.7	533.7	0.13	0.09	0.99

3.2.1. Kinetic triplet for the thermal decomposition

The kinetic analysis of the thermal decomposition involved the calculation of the kinetic triplet, i.e. activation energy (E_a), the kinetic function ($g(\alpha)$), and the pre-exponential factor (A) for the decomposition of the pseudo-components of the SCG.

As shown in the thermogravimetric thermograms, the decomposition of the hemicellulose, cellulose and lignin coincide in a given temperature range and are overlapped to a certain extent. In such situations, auxiliary deconvolution modelling strategies help evaluate the pseudo-components' decomposition and define the individual modelled processes with their particular mass loss and temperature ranges. Although several symmetric and asymmetric functions were explored, Lorentz functions with a symmetric shape better represented the obtained experimental behaviour. The multi-peak fitting strategy for the DTG curves at 2, 5, 10, 15, and 20 °C·min^{-1} resulted in high-reliability values of R^2 above 0.98. For demonstration purposes, the modelling of the experimental results at 2 °C·min^{-1} is shown in **Figure 3a**, where five different peaks were identified, corresponding to moisture, hemicellulose, cellulose, lignin and char. The deconvolutions for the other heating rates are plotted in **Figure S2** of the Supplementary Material. While deconvolution of the peaks for the hemicellulose, cellulose and lignin could be easily performed for all the applied heating rates, the char decomposition could be conveniently evaluated particularly at lower heating rates such as 2, 5 or 10 °C·min^{-1}. Higher heating rates reduced the intensity and widened the appearance of the DTG peak for the char volatilisation, which has been reported to affect the competitive pathway between the endothermic reactions of the primary biomass

decomposition to volatile compounds and the vapour-solid interactions that lead to secondary char formation [95].

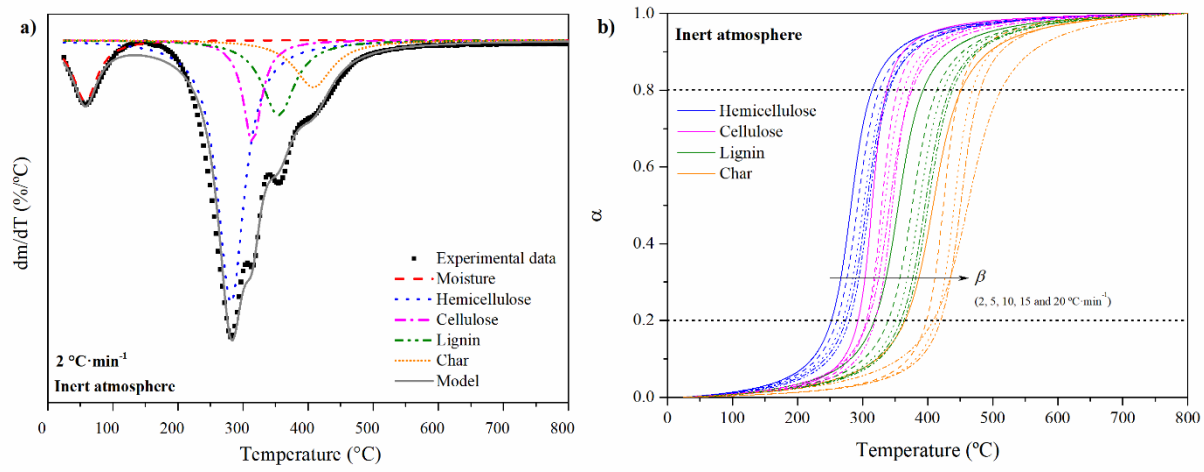

Figure 3. Lorentz-modelling of the thermogravimetric experimental results at a heating rate (β) of 2 °C·min^{-1} (**a**) and individual decomposition process for the pseudo-components and char at all heating rates (**b**) under an inert atmosphere.

After deconvolution, integration allowed obtaining the relative contribution of each pseudo-process, as shown in **Figure 3b**. Subsequently, the iso-conversional methods proposed by Friedman, Flynn-Wall-Ozawa (FWO), and Kissinger-Akahira-Sunose (KAS) were applied as a function of the conversion degree (α). From a global perspective, the induction period happens below 250 °C, while above 400 °C, the complex decomposition of char takes place. Besides these complex regions, given the overlapping decomposition of the different pseudo-components in their initial and/or end stages, avoiding the analyses in such conflictive areas may allow for higher reliability. Therefore, the investigation was focused on the region where the conversion curves exhibit a virtual parallel shift towards higher temperatures when the heating rate increased (α from 0.2 to 0.8), as indicated in **Figure 3b**.

Figure 4 shows the linearized plots for hemicellulose, cellulose, lignin and char for the three iso-conversional methods. The activation energy (E_a) at each conversion degree was determined considering the slopes of the tendency lines drawn for each set of points at different heating rates. The calculated E_a values are plotted in **Figure 5** as a function of the conversion degree. The representation of E_a shows progressive decreasing or increasing linear variations as a function of the conversion degree. First, the

E_a revealed a slightly increasing tendency for the hemicellulose, followed by a smooth linear decreasing behaviour for the cellulose, and a tiny growing performance for lignin, while for char it first slightly increased and then decreased. The variation of activation energy with conversion has been reported before for SCG [31] and other lignocellulosic biomass [96–99] and can be justified by the different chemical reactions that occur during the decomposition of a given pseudo-component, which are dependent on the temperature and, therefore, may be altered with the advance of conversion, resulting in a multi-step reaction. Moreover, the coupling and cooperation of the decomposition processes for the different pseudo-components can determine such variation. Indeed, Brachi *et al.* recently reported the coexistence and competition of heat transfer, chemical transfer and mass transfer that results in a sequential combination of competitive, independent or cooperative phenomena during SCG pyrolysis [31]. Complementarily, the iso-conversional methods adopted for calculating E_a depend on the selected decomposition temperature ranges, which are not constant with β. Indeed, observing **Figure 4**, one can see that for hemicellulose and lignin, the degradation temperature ranges become broader when decreasing the heating rate, while for cellulose, the degradation temperature ranges become narrower for lower heating rates. Considering that each tendency line corresponds to a value of α, for the cellulose, the slope decreases from $\alpha_{0.2}$ to $\alpha_{0.8}$ resulting in a lower value of E_a, while for the hemicellulose and lignin, the slope increases from $\alpha_{0.2}$ to $\alpha_{0.8}$ implying a higher value of E_a.

The average values of apparent activation energy for the different components calculated with the Friedman, FWO and KAS methods together with the mean value are gathered in **Table 7**. The mean value of E_a for the hemicellulose was around 217 kJ·mol^{-1}, which remains within the range of the reported values in the literature [50,100,101]. For the cellulose, the mean value of E_a was around 214 kJ·mol^{-1} and complied with the published values for cellulose decomposition under pyrolytic conditions, ranging between 195 and 235 kJ·mol^{-1} [102,103]. Furthermore, lignin revealed an average E_a of 151 kJ·mol^{-1}, aligned with different sources that reported values between 130−160 kJ·mol^{-1} [104–106]. Finally, E_a for char was around 152 kJ·mol^{-1}. These results were also coherent with those given for the pyrolysis of SCG calculated considering the study of conversion for the whole thermochemical process

[31]. Other studies evaluating the pyrolytic process as a whole also revealed comparable results and demonstrated the possibilities of reducing the activation energy for the pyrolysis of SCG applying, for instance, a torrefaction procedure [32].

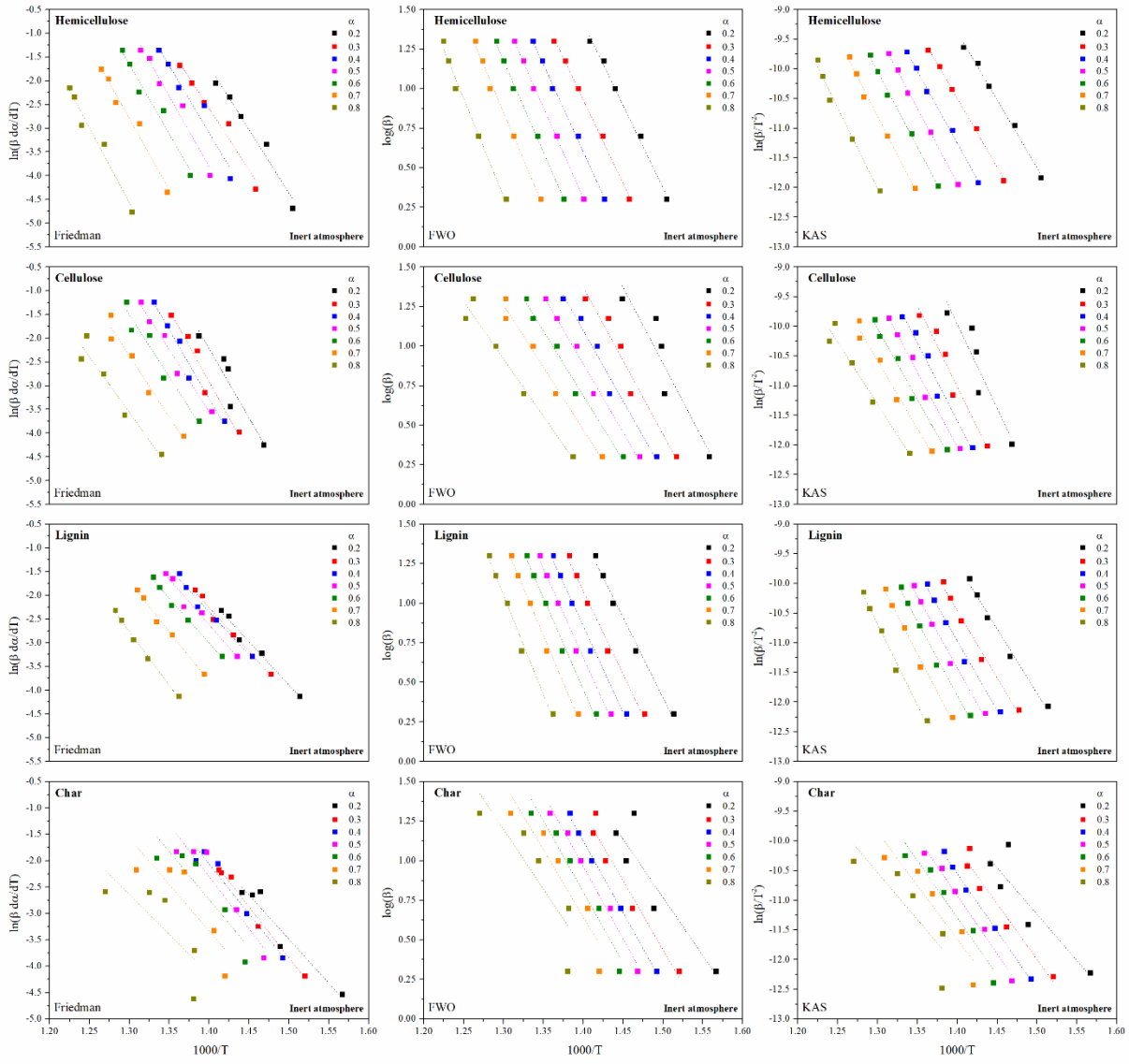

Figure 4. Friedman, FWO and KAS fitting plots of hemicellulose, cellulose, lignin and char for different α under an inert atmosphere.

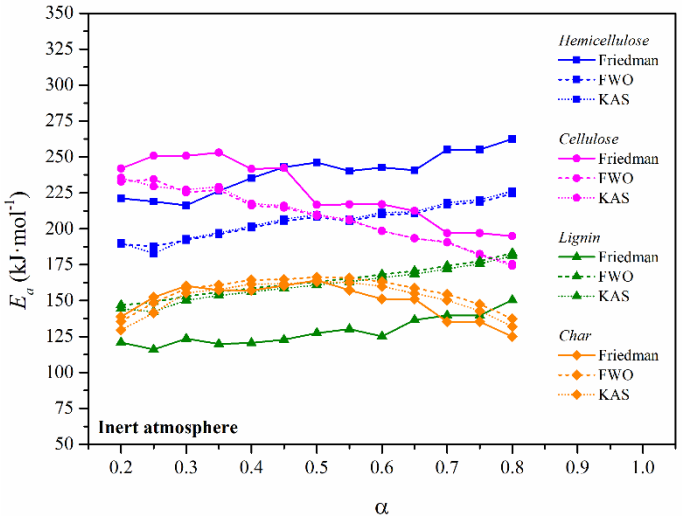

Figure 5. Evolution of apparent activation energy in the range of α from 0.2 to 0.8 calculated with different iso-conversional methods for the hemicellulose, cellulose, lignin and char under an inert atmosphere.

Table 7. Average values for the activation energy (E_a) obtained with the different iso-conversional methods for hemicellulose, cellulose, lignin and char under an inert atmosphere.

	Friedman		**FWO**		**KAS**		***E*$_a$*-mean*** **(kJ·mol^{-1})**
	***E*$_{aFriedman}$** **(kJ·mol^{-1})**	***R*^{2}*-mean***	***E*$_{aFWO}$** **(kJ·mol^{-1})**	***R*^{2}*-mean***	***E*$_{aKAS}$** **(kJ·mol^{-1})**	***R*^{2}*-mean***	
Hemicellulose	239 ± 12	0.97	205 ± 9	0.99	206 ± 10	0.99	217 ± 15
Cellulose	226 ± 20	0.94	208 ± 16	0.96	208 ± 16	0.96	214 ± 8
Lignin	129 ± 8	0.98	164 ± 9	0.99	161 ± 9	0.99	151 ± 15
Char	150 ± 10	0.86	156 ± 9	0.90	152 ± 10	0.91	152 ± 2

The evaluation of the kinetic models for the thermal decomposition was focused on the SCG pseudo-components, i.e. hemicellulose, cellulose and lignin. First, a graphical evaluation was carried out using reduced Master Plots. **Figure 6** shows the experimental curves at a heating rate of 10 °C·min^{-1} (circles) along with the theoretical *g(α)/g(0.5)* curves for the typical decomposition models of biomass (lines). It was observed that all the thermal decomposition reactions were equivalent to the curve of F_n or D_n types. A model between F_3 and F_4 was considered for the hemicellulose, while for the lignin it was selected the F_2 model. However, difficulties were found when assigning the model for the cellulose. The experimental curve moved from a clear D_3 pattern at low conversion to approaching F_3 models at conversion above 0.7. In this regard, it is important to remark that, although the DTG curves were precisely deconvoluted, the decomposition of hemicellulose and cellulose occurs certainly overlapped

in a region that encompasses 75 ºC, involving overlying up to conversions of 0.7 for cellulose. At low and mid conversion for cellulose, the D_3 model may involve a solid-state process in which three-dimensional diffusion happens between crystal lattices or with molecules that must permeate into lattices where motion is restricted, altogether assuming spherical solid particles [86]. In diffusion-controlled reactions, the rate of product formation decreases proportionally with the thickness of the product barrier layer. A product layer may increase where the reaction rate is controlled by the movement of the reactants to or products from the reaction interface. Certainly, at conversions over 0.7, where hemicellulose was completely decomposed, the F_3 model describes the solid-state process for cellulose in which random nucleation with three nuclei on the individual particle can be understood. The F_n models describe solid-state processes in which random nucleation with one, two, or three nuclei on the individual particle occurs. Particularly, nucleation is the formation of a new product phase at reactive points (nucleation sites) in the lattice of the reactant. Thus, the thermal decomposition of a solid produces a new product and a gas at the nucleation sites of the initial reactant. The new nucleation sites grow, and the growth rate could follow an order which depends on the type and nature of the solid reactants [107]. In F_n models, the reaction rate is proportional to the concentration, amount or fraction remaining of reactant(s) raised to a particular power (integral or fractional) which is the reaction order [86].

Even though the above-mentioned deviation was found in the reduced Master Plots for the thermal decomposition of cellulose at higher α, the D_3 was the model with the best correlation, in line with what has been reported when assessing coffee silver skin cellulose's pyrolytic decomposition [50]. Other studies dealing with spent coffee grounds jointly assessed the decomposition of hemicellulose/cellulose as a single stage and assigned an F_3 model [40]. Altogether, for the models assigned in this work, good compliance with the literature was found, where the decomposition of lignocellulosic biomass components under inert conditions is identified as F_n or D_n type, with variations according to the kind of biomass [40,50,108,109].

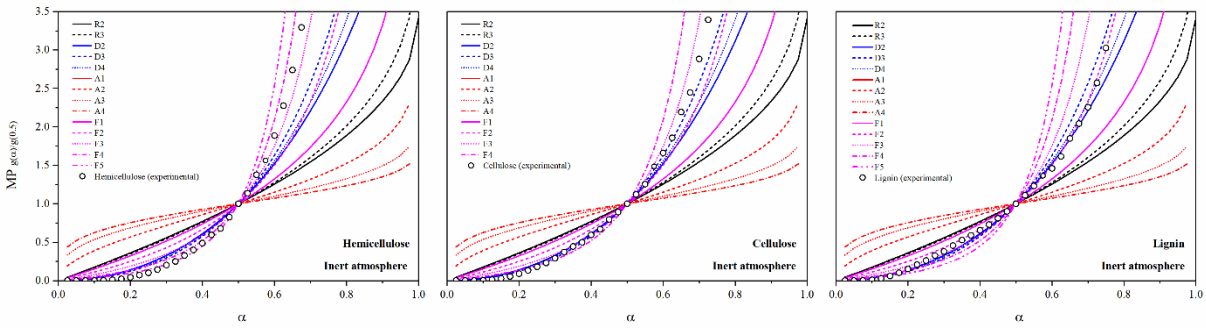

Figure 6. Reduced Master Plots (lines) compared to the experimental decomposition process (circles) of hemicellulose, cellulose and lignin at a heating rate of 10 °C·min^{-1} under an inert atmosphere.

After the evaluation of the thermal decomposition procedure, the pre-exponential factor *A* was approximated using the Coats-Redfern equation (**Equation 12**), and the optimal analytical *n* was estimated for each pseudo-component. **Figure 7** shows the plot of the ln $\left(\frac{\beta\, g(\alpha)}{T^2}\right)$ vs. $\frac{1000}{T}$ at different heating rates for hemicellulose, cellulose and lignin. The straight lines anticipated by the Perez-Maqueda criterion confirm the appropriate fitting of selected models for hemicellulose (F_4), cellulose (D_3) and lignin (F_2).

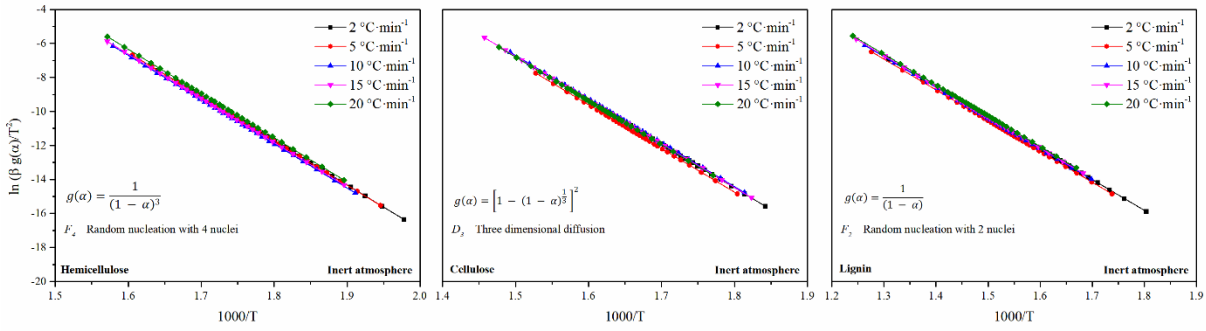

Figure 7. Application of the Perez-Maqueda et al. criterion for the simplified kinetic triplet of hemicellulose, cellulose and lignin at a heating rate equal to 2, 5, 10, 20, 30 °C·min^{-1} under an inert atmosphere.

Table 8 gathers the values for the Napierian logarithm of pre-exponential factor (Ln(*A*)), calculated from the average of A_β at the different heating rates (β), considering the most appropriate model and analytical order (*n*) for hemicellulose, cellulose and lignin under inert atmosphere. The values of *n* calculated with the regression method corroborate the graphical selection of the reaction models. The obtained results for the pre-exponential factor *A* related to the cellulose and hemicellulose are slightly

lower than in other lignocellulosic biomass, while those of lignin were, to some extent, higher [110]. Overall, the obtained error (*e*), which represents the average of absolute deviations from the mean in each set of Ln(A_β) is very low, which validates the considered approach for assessing the kinetic triplet.

Table 8. Frequency factor *A*, reaction model, and analytical reaction order calculated by applying the Perez-Maqueda criterion for hemicellulose, cellulose, and lignin under an inert atmosphere.

	Ln(*A*)	***e* (%)**	***n-MP***	***R*²**	***n-analytical***
Hemicellulose	45.2	0.2	F_3-F_4	0.989	3.7
Cellulose	41.9	0.2	D_3	0.998	-
Lignin	26.6	0.3	F_2	0.970	2.3

3.3. Thermo-oxidative decomposition under oxidative conditions

The thermo-oxidative decomposition of SCG was simulated through thermo-oxidative stability analyses using dynamic experiments at different heating rates in an oxidative atmosphere. The obtained thermogravimetric curves (TG) and their first derivative traces (DTG) are shown in **Figure 8**. From these thermograms, the onset and endset degradation temperatures (T_o, T_e), the peak temperature (T_p), and the mass loss percentages for each stage (Δm) were obtained, and values are gathered in **Table 9**.

Table 9. Onset and endset degradation temperatures (T_o, T_e), residue (R) and peak temperature (T_p) and mass loss percentages for the different noticeable decomposition stages (Δm) obtained at β 2, 5, 10, 15 and 20 °C·min^{-1} under an oxidative atmosphere.

β (°C·min^{-1})	**Water**		**Hemicellulose + cellulose**		**Lignin**		**Char**		***R***	***T_o***	***T_e***
	T_{po} **(°C)**	***Δm_o*** **(%)**	***T_{p1}*** **(°C)**	***Δm_1*** **(%)**	***T_{p2}*** **(°C)**	***Δm_2*** **(%)**	***T_{p3}*** **(°C)**	***Δm_3*** **(%)**	**(%)**	**(°C)**	**(°C)**
2	59.9	5.8	272.7	55.7	401.2	20.0	452.7	16.6	2.0	240.7	468.3
5	70.6	6.3	286.4	55.1	418.9	21.4	480.3	15.9	1.4	252.6	499.2
10	81.8	6.0	294.0	56.8	424.9	21.8	513.0	13.9	1.1	256.0	529.7
15	93.9	5.0	297.0	56.6	443.5	23.8	548.9	13.0	1.0	264.1	562.4
20	91.4	7.5	301.7	55.2	450.1	22.3	559.6	14.2	0.5	267.0	572.9

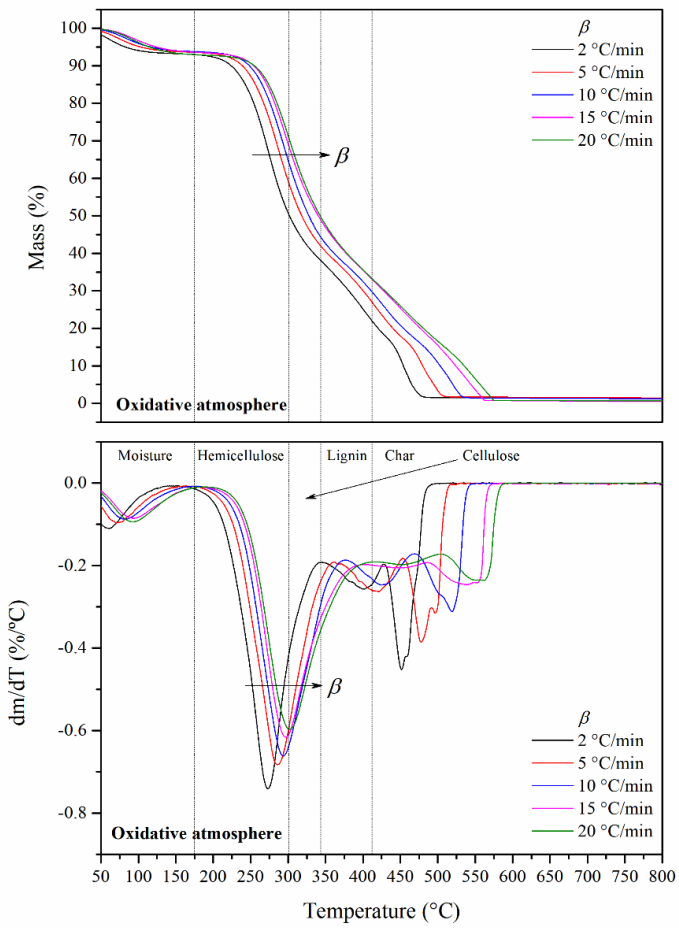

Figure 8. Thermogravimetric thermograms (TG) and their first derivative traces (DTG) of SCG under an oxidative atmosphere at β 2, 5, 10, 15, 20 °C·min^{-1}.

During heating, mass progressively decreased, revealing the presence of the mass loss regions of decomposition of biomass pseudo-components. The initial mass reduction, with a contribution of ~6% from 25 °C to 150 °C, is related to the moisture vaporisation, in line with results obtained using an inert atmosphere. This stage is followed by the joint devolatilization of hemicellulose and cellulose with a mass loss of ~55% between 170 °C and 350 °C. The overlapping of hemicellulose and cellulose decomposition can be visually perceived in the DTG curves as a prominent peak with a shoulder at high temperatures. Subsequently, lignin decomposition was identified between 350 °C and 450 °C, with a ~20% mass loss. The last process above 425 °C with a ~15% mass loss was ascribed to the decomposition of char. After that, the mass loss increases quickly until temperatures of 550–650 °C, up to virtually complete volatilisation. The minor residue (*R*) at the end of the analysis with a mass loss

percentage below 2% may be attributed to the remnant ash. These values are in concordance with the ash percentage reported in the proximate analysis of SCG.

As expected, heating rate variations affected both the TGA curve's shape and the DTG peaks. Increasing the heating rate displaced all the curves and characteristic decomposition temperatures towards higher values, as shown in **Figure 9** for the onset, endset, and peaks for hemicellulose and cellulose (T_{p1}), lignin (T_{p2}) and char (T_{p3}). The zero-decomposition temperature (*ZDT*) for a virtually null heating rate was calculated, together with the fitting parameters *a*, *b* and *k*, all gathered in **Table 10**, with R^2 values above 0.97. When β tends to zero, the onset temperature for the volatilisation of SCG was 232 °C, the decomposition of the hemicellulose and cellulose became at 261 °C, that of lignin at 389 °C, with the char decomposing at 431 °C, reaching the endset of the process at 446 °C.

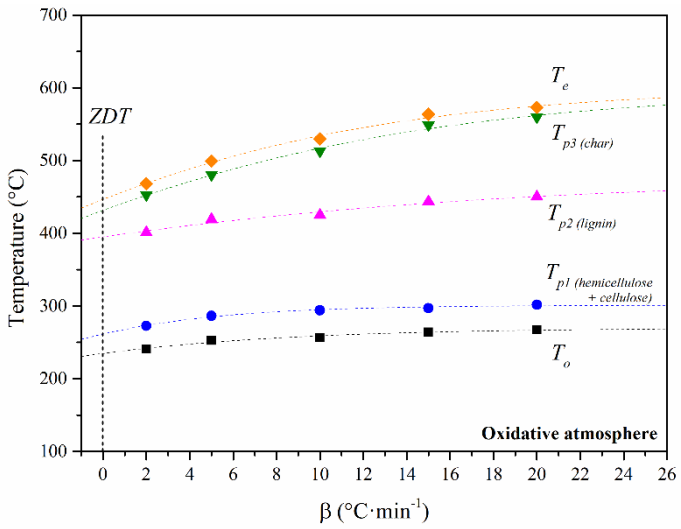

Figure 9. Evolution of the characteristic decomposition temperatures T_o, T_e, $T_{p1\ (hemicellulose+cellulose)}$, $T_{p2\ (lignin)}$, and $T_{p3\ (char)}$ at β of 2, 5, 10, 15, 20 °C·min^{-1} under an oxidative atmosphere.

Table 10. ZDT values ($\beta \rightarrow 0$) along with the fitting parameters (a, b and k) and regression coefficients for the onset (T_o), endset (T_e), hemicellulose+cellulose (T_{p1}), lignin (T_{p2}) and char (T_{p3}) decomposition temperatures under an oxidative atmosphere.

	ZDT ***(β → 0)*** **(°C)**	***a***	***b***	***k***	**R^2**
Onset (T_o)	232.3	268.0	0.15	0.16	0.97
Hemicellulose+cellulose (T_{p1})	261.1	300.9	0.15	0.20	0.97
Lignin (T_{p2})	389.1	459.0	0.17	0.10	0.98
Char (T_{p3})	431.5	597.6	0.39	0.09	0.99
Endset (T_e)	446.6	600.9	0.35	0.10	0.99

3.3.1. Kinetic triplet for the thermo-oxidative decomposition

Concerning the kinetic triplet, the activation energy, the kinetic function *g(α),* and the pre-exponential factor were ascertained. As studied in an inert atmosphere, the kinetic analysis's conversion degree (α) was selected in the range of 0.2–0.8 to avoid heterogeneous initiation and end-stage reactions. Thanks to the deconvolution analysis shown in **Figure 10a** for 2 ºC·min^{-1} and in **Figure S3** of the Supplementary Material for the other heating rates, the peaks related to pseudo-components and char were defined, the individual conversion curves were gained through integration, as shown in **Figure 10b**, and their activation energy was estimated.

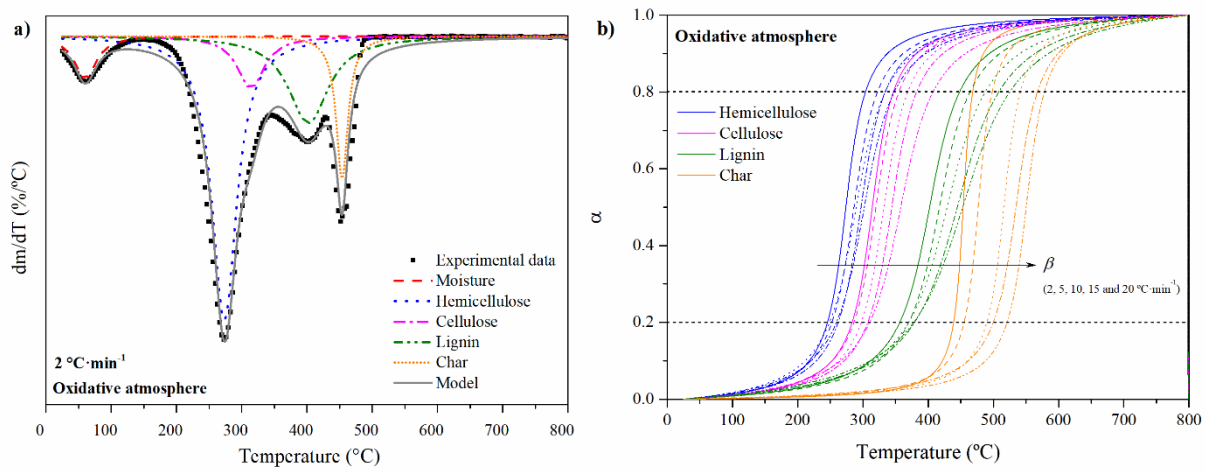

Figure 10. Lorentz-modelling of the thermogravimetric experimental results at a heating rate (β) of 2 °C·min^{-1} (**a**) and individual decomposition process for the pseudo-components at all heating rates (**b**) under an oxidative atmosphere.

Figure 11 shows the linearized plots for hemicellulose, cellulose, lignin and char for the three iso-conversional methods (Friedman, FWO and KAS). The activation energy (E_a) at each conversion degree (α) was gained from the slopes of the tendency lines at different heating rates, which showed a degree of correlation (R^2) above 0.95 in the selected α range. Only for hemicellulose at a lesser conversion degree (α) of 0.2−0.3, lower R^2 between 0.65 and 0.90 was found due to initiation reactions, while for char R^2 between 0.74 and 0.94 was found when applying the Friedman method, especially low for high conversion, when termination reactions occur.

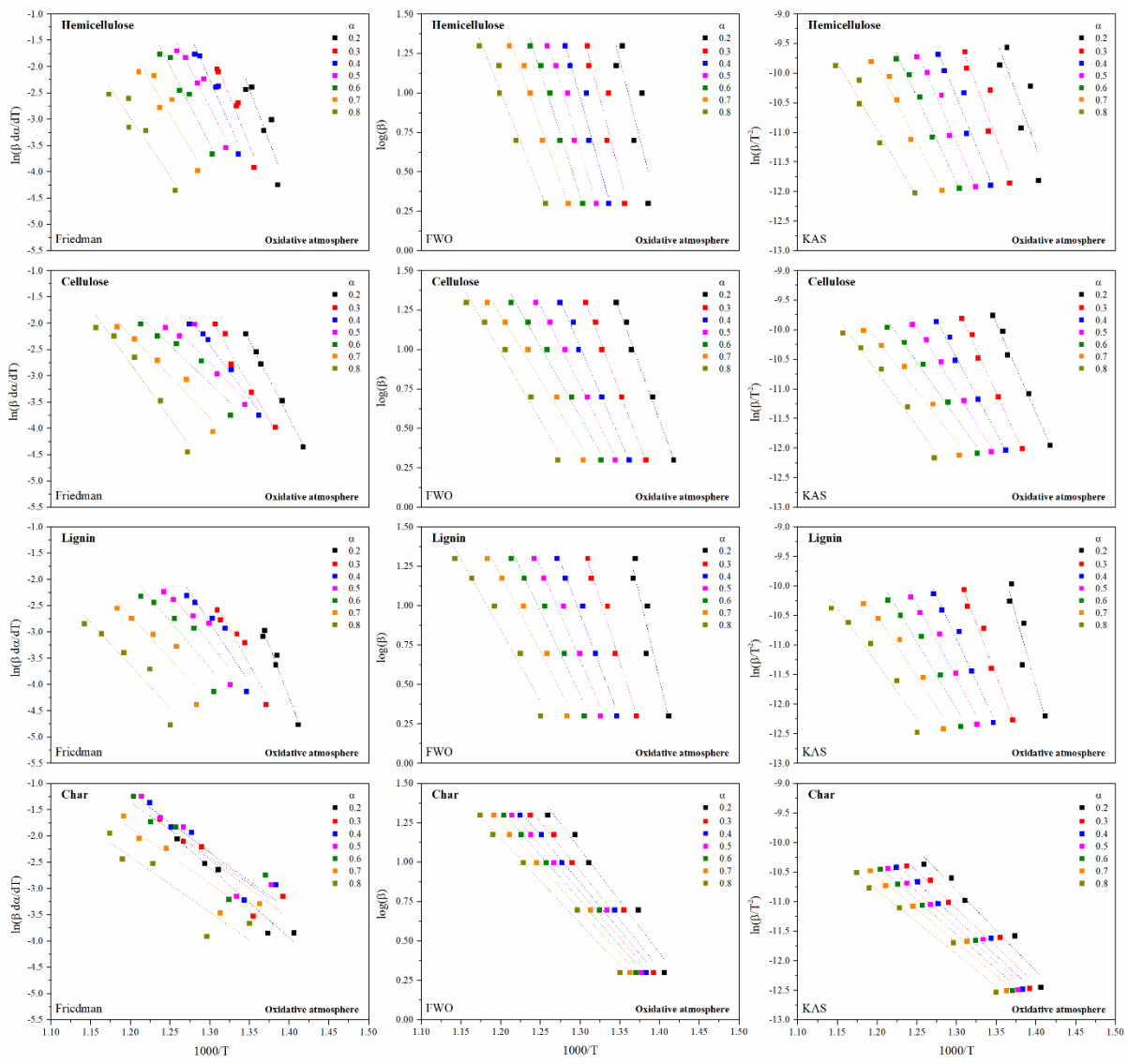

Figure 11. Friedman, FWO and KAS fitting plots of hemicellulose, cellulose, lignin and char for different α under an oxidative atmosphere.

The apparent E_a is plotted in **Figure 12** as a function of the conversion degree. A non-constant behaviour with a generally decreasing outline was obtained with the advance of the conversion degree. Reasonably, when conversion increased, highly oxidised pseudo-component units resulted in decomposition with lower activation energy. Moreover, it can also contribute to the autocatalytic effect from heat released during the chemical recombination of by-products generated during degradation, at the solid-gas interface or within the solid matrix, which may increase the local temperature in the solid and enhance decomposition [111]. Slight differences arise for the three calculation methods connected to their differential (Friedman) or integral nature (FWO and KAS), ascribed to numerical differentiation [90]. The average values of apparent activation energy for the hemicellulose, cellulose, lignin and char are gathered in **Table 11**. Although they mostly coincide with those reported in the literature, some differences were found considering the study of dissimilar types of biomass. The achieved results for the hemicellulose with a mean E_a of 194 kJ·mol^{-1} are comparable to those reported for the oxidation stage of pure hemicellulose [112] but slightly above other values described for other biomass such as persimmon harvest [110] or pinewood waste [101]. For cellulose, a mean E_a of 147 kJ·mol^{-1} comply results presented in other works dealing with pure cellulose [112] and other biomass such as persimmon stems [110], rice straw [90] or olive oil solid waste [113]. The mean E_a value of lignin is around 174 kJ·mol^{-1}, in line with what was found when assessing pure lignin [112]. Other studies found lower E_a for lignin, but one must consider the particular biomass type and the deconvolution analysis conditions. Particularly for lignin in SCG, and considering that its decomposition occurs in a wide temperature range, it must be recognised that this process may be overlapped with other simultaneous secondary reactions of intermediate by-products generated during the decomposition of hemicellulose, cellulose and other minor components [114], which will subsequently determine its apparent activation energy. Finally, the E_a value of char was close to 100 kJ·mol^{-1}.

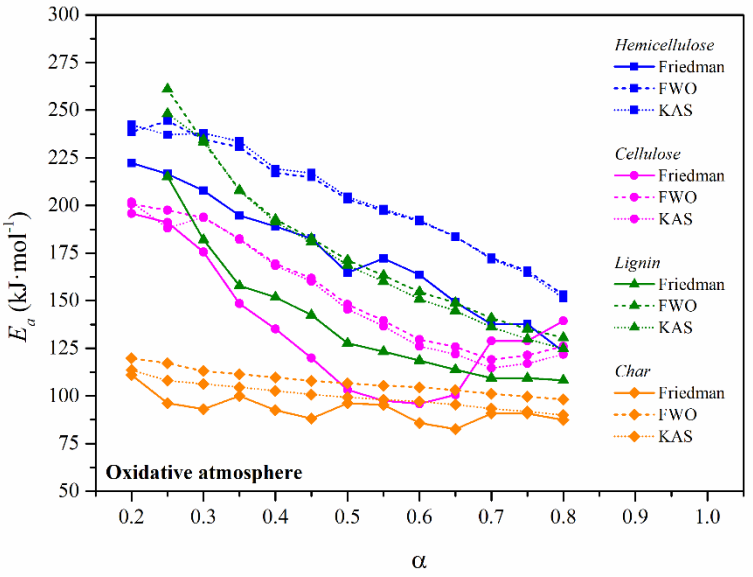

Figure 12. Evolution of apparent activation energy in the range of α from 0.2 to 0.8 calculated with different iso-conversional methods for the hemicellulose, cellulose, lignin and char under an oxidative atmosphere.

Table 11. Average values for the activation energy (E_a) obtained with the different iso-conversional methods for hemicellulose, cellulose, lignin and char under an oxidative atmosphere.

	Friedman		FWO		KAS		E_a-mean (kJ·mol^{-1})
	$E_{aFriedman}$ (kJ·mol^{-1})	R^2-mean	E_{aFWO} (kJ·mol^{-1})	R^2-mean	E_{aKAS} (kJ·mol^{-1})	R^2-mean	
Hemicellulose	174 ± 26	0.92	204 ± 24	0.95	204 ± 25	0.94	194 ± 13
Cellulose	135 ± 27	0.95	156 ± 27	0.99	152 ± 28	0.99	148 ± 8
Lignin	148 ± 35	0.90	187 ± 41	0.97	184 ± 42	0.96	173 ± 17
Char	93 ± 5	0.89	108 ± 5	0.98	100 ± 5	0.98	100 ± 5

The most appropriate kinetic model was graphically evaluated for the SCG pseudo-components using reduced Master Plots. **Figure 13** illustrates the experimental curves at a heating rate of 10 °C·min^{-1} with the theoretical *g(α)* curves. All the reaction pathways were comparable to the curves of the F_n type ascribed to random nucleation being *n* the number of nuclei or to the D_3 type, in which three-dimensional diffusion happens. An F_4 model was selected for hemicellulose. For cellulose, the D_3 type was established [115]. The lignin decomposition occurred following a model between the F_3 and F_4, with a better correlation to the F_4 type. These results are consistent with other studies in the literature dealing with the oxidative decomposition of lignocellulosic biomass [90,110,115,116].

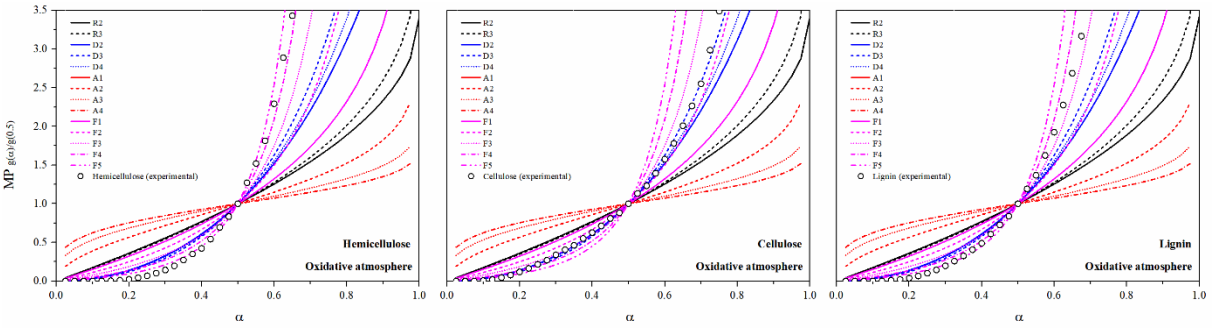

Figure 13. Reduced Master Plots (lines) compared to the experimental decomposition process (circles) of hemicellulose, cellulose and lignin at a heating rate of 10 °C·min^{-1} under an oxidative atmosphere.

Afterwards, the pre-exponential factor *A* was calculated using the Coast-Redfern equation, and the optimal analytical *n* was estimated for each pseudo-component. **Figure 14** shows the plot of the ln $\left(\frac{\beta\, g(\alpha)}{T^2}\right)$ vs. $\frac{1000}{T}$ at different heating rates for hemicellulose, cellulose and lignin. The application of the Perez-Maqueda *et al.* criterion confirmed the proper selection of $g(\alpha)$ and models for hemicellulose (F_4), cellulose (D_3) and lignin (F_4).

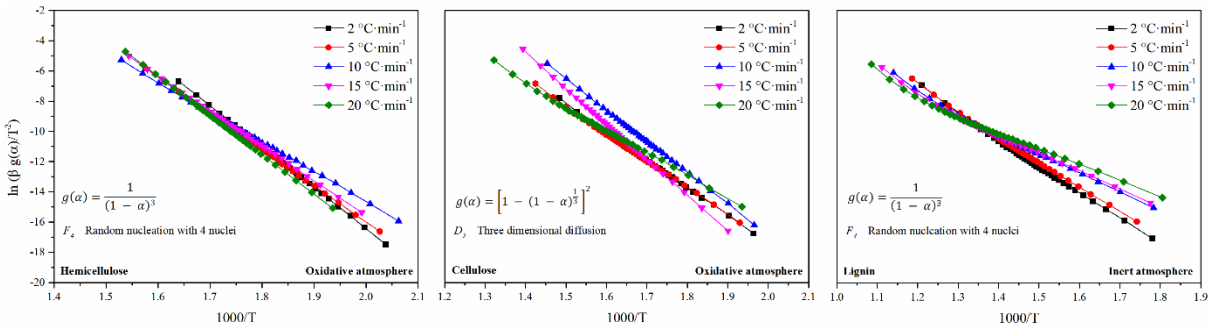

Figure 14. Application of the Perez-Maqueda et al. criterion for the simplified kinetic triplet of hemicellulose, cellulose, and lignin at a heating rate of 2, 5, 10, 20, 30 °C·min^{-1} under an oxidative atmosphere.

Table 12 gathers the values for the pre-exponential factor, calculated as an average between the A_β at the different heating rates and the calculated analytical order *n* for hemicellulose, cellulose and lignin under an oxidative atmosphere. The obtained results for the pre-exponential factor *A* are in the same magnitude as those reported for lignocellulosic biomass [90]. Only the one corresponding to lignin

shows slightly greater values of *A*, given its high dependence on the activation energy. The analytical calculation of *n* confirmed the reaction path selected in the graphical Master Plots.

Table 12. Frequency factor *A*, reaction model, and analytical reaction order calculated by applying the Perez-Maqueda criterion for hemicellulose, cellulose and lignin under an oxidative atmosphere.

	Ln(*A*)	***e* (%)**	***n-MP***	R^2	***n-analytical***
Hemicellulose	41.9	3.0	F_4	0.999	3.7
Cellulose	28.3	1.5	D_3	0.999	-
Lignin	28.6	0.4	F_4	0.997	3.6

3.4. Thermal vs thermo-oxidative decomposition

In this section, the similarities and differences between the thermochemical process undergone in both inert and oxidative atmospheres are highlighted. First, the evaluation of the zero-decomposition temperature (*ZDT*) plotted in **Figure 15a** demonstrated that both the onset and endset of the main mass loss stage and the peak temperatures for the pseudo-components were generally lower under an oxidative atmosphere, regardless of the heating rate. The contribution of oxidation reactions promoted the generation of oxy-cellulosic materials in the SCG that decompose with the evolution of water, carbon monoxide and carbon dioxide, together with the generation of carbonyl and carboxyl species that contribute to accelerating degradation. Therefore, heating under an oxidative atmosphere results in a combination of hydrolysis, oxidation, and thermal decomposition, which subsequently promotes rapid and complete degradation of the SCG. The virtually null percentage of the ash residue at the end of the thermo-oxidative reaction must be highlighted, which points out the convenience of using SCG for combustion reactions.

However, the pyrolytic process under an inert atmosphere resulted in thermal decomposition reactions involving chain breakages, molecular weight reduction, and recombination of chemical bonds to form new volatile (H_2O, CO_2, CO and CH_4), bio-oils (alcohols, esters, hydrocarbons and acids), and solid compounds, such as the generated biochar at the end of the process, with a mass percentage of nearly 20% of the original biomass [32,38,40]. Biochar is a carbon-rich, porous solid produced after the partial thermochemical decomposition of biomass after the elimination of volatile compounds such as gases,

oils and tar, and it can contain carboxylates or salts of carboxylic acids and silicates [47]. The microscopic surface of the biochar usually shows a micro-, meso- and macroporous carbon matrix structure with a large specific surface area, active functional groups and high pH. These features give biochar an excellent potential for being used as organic and inorganic pollutants adsorbent [117] or catalyst for biofuel production [118], especially after being physically or chemically activated. It can also be used as a soil conditioner to increase soil fertility and quality by increasing pH and microbial activity, modulating moisture retention and improving cation exchange capacity [119]. Furthermore, biochar has a high calorific value, so it can be used in the production of briquettes, an excellent substitute for charcoal, that can be marketed as a household biofuel for fireplaces, stoves and also for powering industrial boilers.

Figure 15b shows the value of E_α for hemicellulose, cellulose and lignin in the two atmospheres, as obtained from the average of the Friedman, FWO, and KAS methods. As expected, the average value of E_a was generally higher in the inert atmosphere than in the oxidative one, as the reaction of the pseudo-components and oxygen speeds up the degradation and decreases the value of the energy barrier. Although the exception of lignin can be mentioned, the calculated average activation energies were similar, considering the deviation from the different calculation methods. Additionally, as mentioned before, lignin decomposition happens in a long temperature range and overlaps with other decomposition and secondary reactions. This behaviour may promote difficulties in deconvolution, especially at a low conversion degree, where a high E_a for lignin was found under an oxidative atmosphere. From a general perspective, the obtained apparent activation energies were aligned with typical values of lignocellulosic biomass, as discussed in previous sections.

As for the E_a evolution with conversion shown in **Figure 15d**, under an inert atmosphere, E_a rises during the decomposition of hemicellulose, which describes the competitive nature of the process, and suggests that the hemicellulose degradation path occurs through the random breaking of certain bonds of the branched structure inside a cellulose and lignin polymeric matrix. Then it slightly decreased during the degradation of cellulose. The E_a reduction with conversion has been ascribed to the cellulose activation

during the pyrolysis, which reduced its degree of polymerisation and subsequently the E_a value [50]. Other authors for different lignocellulosic biomass also found that E_a can remain constant during conversion, which is ascribed to the absence of cooperative phenomena, suggesting that pyrolytic degradation occurs on energetically equivalent intra or inter-particle bonds [58]. Finally, the E_a for lignin increase again, as it has a complex structure, more difficult to decompose than cellulose, showing that the kinetic parameters and reaction mechanism strongly depend on the conversion degree, typical of multi-step reactions [120,121]. This behaviour was found in other studies dealing with the pyrolytic decomposition of lignocellulosic biomass [32,40,68,107]. For the case of SCG, this overall E_a variation profile pointed out the pyrolytic decomposition as a multi-step reaction with the absence of autocatalytic reactions [58].

Conversely, during decomposition under thermo-oxidative conditions, a non-constant decreasing profile of E_a was obtained with the advance of the conversion degree for all the pseudo-components. When conversion increased, highly oxidised units of biomass resulted in decomposition with lower activation energy, together with the autocatalytic effect from heat released during the chemical recombination of by-products generated during degradation, at the solid-gas interface or within the solid matrix, which may increase the local temperature in the solid and enhance decomposition [111].

Figure 15c displays the values of the frequency factor (A) in the logarithmic scale of hemicellulose, cellulose, and lignin under inert and oxidative atmospheres. The frequency factor describes the rate of molecular collisions that occur in the chemical reaction. It is generally obtained experimentally to ensure that the chemical reaction parameters (temperature, activation energy, and constant rate) conform to the form of the Arrhenius equation. When the value of A is higher, it indicates a greater molecular collision, which in turn requires more heat to be transferred because of the higher activation energy [122]. Given the strong dependence of A on the activation energy, a similar pattern was found, being generally higher under inert than oxidative atmospheres. The pseudo-components hemicellulose, cellulose and lignin possessed a higher frequency factor the lower the temperature of their decomposition process, as found

before for other lignocellulosic biomasses [110,123]. This is probably due to the greater energy demand in the initiation stages for decomposing hemicellulose and cellulose.

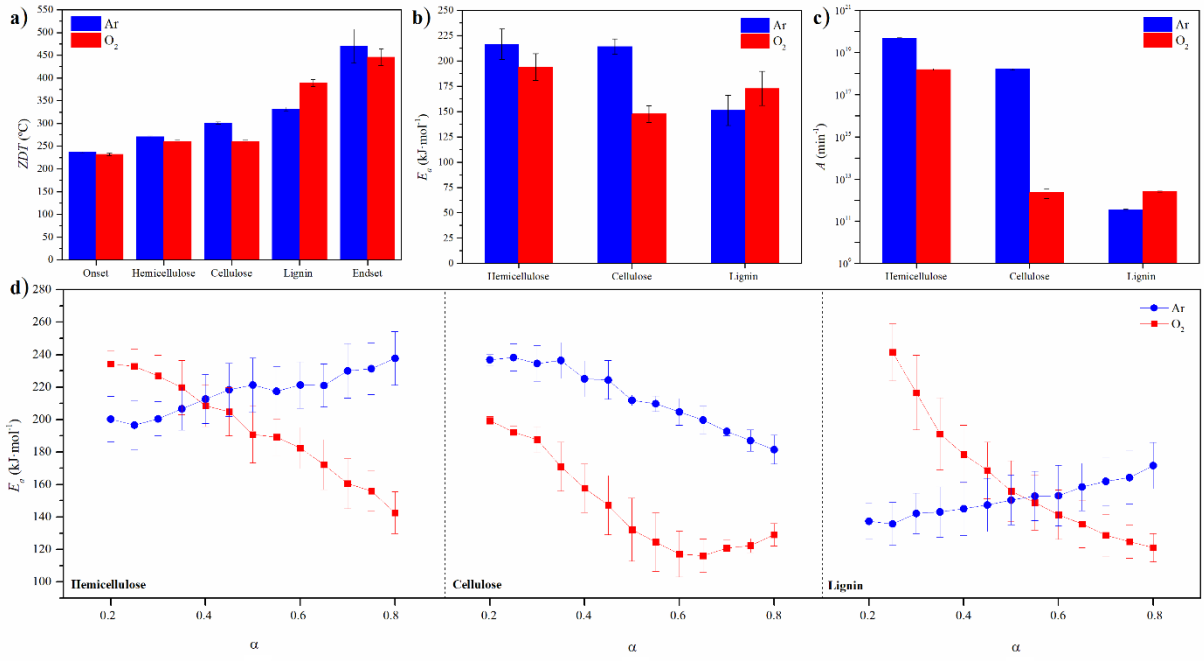

Figure 15. **(a)** Zero decomposition temperature (*ZDT*), **(b)** Average activation energy (E_a), **(c)** Frequency factor (A) and (**d**) Evolution of E_a with the conversion of hemicellulose, cellulose and lignin under inert and oxidative atmospheres.

Finally, **Table 13** summarises the reaction model, the kinetic function $g(\alpha)$ and the analytical reaction order calculated by applying the Perez-Maqueda criterion for hemicellulose, cellulose and lignin under inert and oxidative atmospheres. In general, similar decomposition modes were found regardless of the atmosphere for hemicellulose (F_4), hemicellulose (D_3), and lignin ($F_{2/4}$), which proposes that the gas atmosphere may not define their reaction pathway. Instead, this observation suggests that the temperature, the reactant concentration, the particle shape and the diffusion of degradation products indeed control the decomposition of SCG during non-isothermal pyrolytic or combustive processes. Models applied to solid-state kinetics can be classified according to their mechanistic basis, i.e. nucleation, geometrical contraction, diffusion and reaction order [86].

Table 13. Reaction model, kinetic function g(α) and analytical reaction order calculated by applying the Perez-Maqueda criterion for hemicellulose, cellulose and lignin under oxidative and inert atmospheres.

	Inert			Oxidative		
	n-MP	***n-analytical***	***g(α)***	***n-MP***	***n-analytical***	***g(α)***
Hemicellulose	F_4	3.7	$\frac{1}{(1-\alpha)^3}$	F_4	3.7	$\frac{1}{(1-\alpha)^3}$
Cellulose	D_3	-	$\left[1-(1-\alpha)^{\frac{1}{3}}\right]^2$	D_3	-	$\left[1-(1-\alpha)^{\frac{1}{3}}\right]^2$
Lignin	F_2	2.3	$\frac{1}{(1-\alpha)}$	F_4	3.6	$\frac{1}{(1-\alpha)^3}$

4. Conclusions

Under inert and oxidative atmospheres, the spent coffee grounds (SCG) exhibit thermogravimetric mass-loss curves showing the sequential devolatilization of humidity, hemicellulose, cellulose, lignin and char. Under inert conditions, biochar was generated (~20%), while under an oxidative environment, complete volatilisation occurred. The contribution of oxygen to enhancing the decomposition of SCG regardless of the heating rate was corroborated through the study of the zero-decomposition temperature.

The deconvolution of the thermogravimetric curves allowed for evaluating the particular kinetic triplet for the pseudo-components: hemicellulose, cellulose and lignin. Although activation energy and pre-exponential factors were lower during thermo-oxidative than thermal decomposition, very similar kinetic functions were obtained for hemicellulose (F_4) and cellulose (D_3) regardless of the reaction environment. Lignin, with a more complex decomposition process overlapped with other constituents in a wide temperature range, especially under an inert atmosphere, showed slight differences in the reaction order. Mainly, the F_2 type was identified during pyrolysis and F_4 in an oxidative atmosphere, which demonstrates that the presence of the oxidation agent allows to speed up the reaction. Altogether, the gas atmosphere did not alter the reaction models, suggesting that the reaction path was instead controlled by the temperature, the reactant concentration, the particle shape and the diffusion of degradation products.

The obtained kinetic parameters for the SCG's pseudo-components are crucial for understanding the thermochemical conversion of SCG, conducted through pyrolysis or combustion, and allow gaining

knowledge for extending their valorisation possibilities, for successfully designing and optimizing pyrolysis or combustion reactors, predicting material lifetime, CFD modelling, and establishing process conditions. Overall, the SCG composition rich in carbon and oxygen with low nitrogen and null sulphur content, low ash yield, and high calorific value (LHV and HHV close to 20 $MJ \cdot kg^{-1}$), demonstrated the convenience of using SCG as a renewable source in pyrolytic or combustive thermochemical conversion reactions.

Acknowledgements

The authors would like to thank the Chilean Economic Development Agency (CORFO) for the financial support through project 13CEI2-21839 and the contract for C.T. Primaz. Generalitat Valenciana is also acknowledged for the APOSTD/2020/155 grant for O. Gil-Castell. Finally, O-Gil-Castell wants to dedicate this research to her beloved daughter Alexandra G. M., in commemoration of her birth.

Data availability

The data supporting this study's findings are available from the corresponding author upon reasonable request.

Conflict of interest

The authors declare no conflicts of interest.

References

[1] M.O. Daramola, A.O. Ayeni, Valorization of Biomass to Value-Added Commodities, Springer International Publishing, Cham, 2020. https://doi.org/10.1007/978-3-030-38032-8.

[2] A. Saravanan, P. Senthil Kumar, S. Jeevanantham, S. Karishma, D.-V.N. Vo, Recent advances and sustainable development of biofuels production from lignocellulosic biomass, Bioresour Technol. 344 (2022) 126203. https://doi.org/10.1016/j.biortech.2021.126203.

[3] M.J. Blair, B. Gagnon, A. Klain, B. Kulišić, Contribution of Biomass Supply Chains for Bioenergy to Sustainable Development Goals, Land (Basel). 10 (2021) 181. https://doi.org/10.3390/land10020181.

[4] V. Ashokkumar, R. Venkatkarthick, S. Jayashree, S. Chuetor, S. Dharmaraj, G. Kumar, W.-H. Chen, C. Ngamcharussrivichai, Recent advances in lignocellulosic biomass for biofuels and value-added bioproducts - A critical review, Bioresour Technol. 344 (2022) 126195. https://doi.org/10.1016/j.biortech.2021.126195.

[5] A. Senatore, G. Giorgianni, F. Dalena, E. Giglio, Lignocellulosic biomass conversion into bioenergy: Feedstock overview, Journal of Phase Change Materials. 1 (2021). https://doi.org/10.58256/JPCM.V1I1.7.

[6] P.S. Murthy, M. Madhava Naidu, Sustainable management of coffee industry by-products and value addition - A review, Resour Conserv Recycl. 66 (2012) 45–58. https://doi.org/10.1016/j.resconrec.2012.06.005.

[7] C. V. Garcia, Y.-T. Kim, Spent Coffee Grounds and Coffee Silverskin as Potential Materials for Packaging: A Review, J Polym Environ. 29 (2021) 2372–2384. https://doi.org/10.1007/s10924-021-02067-9.

[8] A.S.C. de Bomfim, D.M. de Oliveira, E. Walling, A. Babin, G. Hersant, C. Vaneeckhaute, M.-J. Dumont, D. Rodrigue, Spent Coffee Grounds Characterization and Reuse in Composting and Soil Amendment, Waste. 1 (2022) 2–20. https://doi.org/10.3390/waste1010002.

[9] M. Hoseini, S. Cocco, C. Casucci, V. Cardelli, G. Corti, Coffee by-products derived resources. A review, Biomass Bioenergy. 148 (2021) 106009. https://doi.org/10.1016/j.biombioe.2021.106009.

[10] S.I. Mussatto, L.M. Carneiro, J.P.A. Silva, I.C. Roberto, J.A. Teixeira, A study on chemical constituents and sugars extraction from spent coffee grounds, Carbohydr Polym. 83 (2011) 368–374. https://doi.org/10.1016/j.carbpol.2010.07.063.

[11] M.A. Silva, S.A. Nebra, M.J. Machado Silva, C.G. Sanchez, The use of biomass residues in the Brazilian soluble coffee industry, Biomass Bioenergy. 14 (1998) 457–467. https://doi.org/10.1016/S0961-9534(97)10034-4.

[12] F. Battista, E.M. Barampouti, S. Mai, D. Bolzonella, D. Malamis, K. Moustakas, M. Loizidou, Added-value molecules recovery and biofuels production from spent coffee grounds, Renewable and Sustainable Energy Reviews. 131 (2020) 110007. https://doi.org/10.1016/j.rser.2020.110007.

[13] W.R. Stahel, The circular economy, Nature 2016 531:7595. 531 (2016) 435–438. https://doi.org/10.1038/531435a.

[14] X.C. Schmidt Rivera, A. Gallego-Schmid, V. Najdanovic-Visak, A. Azapagic, Life cycle environmental sustainability of valorisation routes for spent coffee grounds: From waste to resources, Resour Conserv Recycl. 157 (2020) 104751. https://doi.org/10.1016/j.resconrec.2020.104751.

[15] S.K. Karmee, A spent coffee grounds based biorefinery for the production of biofuels, biopolymers, antioxidants and biocomposites, Waste Management. 72 (2018) 240–254. https://doi.org/10.1016/J.WASMAN.2017.10.042.

[16] M.G. Plaza, A.S. González, C. Pevida, J.J. Pis, F. Rubiera, Valorisation of spent coffee grounds as CO2 adsorbents for postcombustion capture applications, Appl Energy. 99 (2012) 272–279. https://doi.org/10.1016/j.apenergy.2012.05.028.

[17] A. Cervera-Mata, S. Pastoriza, J.Á. Rufián-Henares, J. Párraga, J.M. Martín-García, G. Delgado, Impact of spent coffee grounds as organic amendment on soil fertility and lettuce growth in two Mediterranean agricultural soils, Arch Agron Soil Sci. 64 (2018) 790–804. https://doi.org/10.1080/03650340.2017.1387651.

[18] H. Moustafa, C. Guizani, C. Dupont, V. Martin, M. Jeguirim, A. Dufresne, Utilization of torrefied coffee grounds as reinforcing agent to produce high-quality biodegradable PBAT composites for food packaging applications, ACS Sustain Chem Eng. 5 (2017) 1906–1916. https://doi.org/10.1021/acssuschemeng.6b02633.

[19] P.T.K. Le, Q.T. Vu, Q.T. Nguyen, K.A. Tran, K.A. Le, Spent coffee grounds as a valuable source of bioactive compounds and bioenergy, Chem Eng Trans. 56 (2017) 37–42. https://doi.org/10.3303/CET1756007.

[20] R.J. Martínez, A.Z. Vela-Carrillo, L.A. Godínez, J. de J. Pérez-Bueno, I. Robles, Competitive adsorption of anionic and cationic molecules on three activated carbons derived from agroindustrial waste, Biomass Bioenergy. 168 (2023) 106660. https://doi.org/10.1016/j.biombioe.2022.106660.

[21] M. Stylianou, A. Agapiou, M. Omirou, I. Vyrides, I.M. Ioannides, G. Maratheftis, D. Fasoula, Converting environmental risks to benefits by using spent coffee grounds (SCG) as a valuable resource, Environmental Science and Pollution Research. 25 (2018) 35776–35790. https://doi.org/10.1007/s11356-018-2359-6.

[22] T.M. Mata, A.A. Martins, N.S. Caetano, Bio-refinery approach for spent coffee grounds valorization, Bioresour Technol. 247 (2018) 1077–1084. https://doi.org/10.1016/j.biortech.2017.09.106.

[23] J. Rajesh Banu, S. Kavitha, R. Yukesh Kannah, M. Dinesh Kumar, Preethi, A.E. Atabani, G. Kumar, Biorefinery of spent coffee grounds waste: Viable pathway towards circular bioeconomy, Bioresour Technol. 302 (2020) 122821. https://doi.org/10.1016/J.BIORTECH.2020.122821.

[24] C.-H. Dang, T.-D. Nguyen, Physicochemical Characterization of Robusta Spent Coffee Ground Oil for Biodiesel Manufacturing, Waste Biomass Valorization. 10 (2019) 2703–2712. https://doi.org/10.1007/s12649-018-0287-9.

[25] N.S. Caetano, V.F.M. Silva, A.C. Melo, A.A. Martins, T.M. Mata, Spent coffee grounds for biodiesel production and other applications, Clean Technol Environ Policy. 16 (2014) 1423–1430. https://doi.org/10.1007/s10098-014-0773-0.

[26] N. Kondamudi, S.K. Mohapatra, M. Misra, Spent Coffee Grounds as a Versatile Source of Green Energy, J Agric Food Chem. 56 (2008) 11757–11760. https://doi.org/10.1021/jf802487s.

[27] A.W. Go, T.Y.N. Pham, Y.-H. Ju, R.C. Agapay, A.E. Angkawijaya, K.L. Quijote, Extraction of lipids from post-hydrolysis spent coffee grounds for biodiesel production with hexane as solvent: Kinetic and equilibrium data, Biomass Bioenergy. 140 (2020) 105704. https://doi.org/10.1016/j.biombioe.2020.105704.

[28] T. Vítěz, T. Koutný, M. Šotnar, J. Chovanec, On the spent coffee grounds biogas production, Acta Universitatis Agriculturae et Silviculturae Mendelianae Brunensis. 64 (2016) 1279–1282. https://doi.org/10.11118/actaun201664041279.

[29] P. Basu, Biomass Gasification, Pyrolysis and Torrefaction, Elsevier, 2013. https://doi.org/10.1016/C2011-0-07564-6.

[30] E. Sermyagina, C.L. Mendoza Martinez, M. Nikku, E. Vakkilainen, Spent coffee grounds and tea leaf residues: Characterization, evaluation of thermal reactivity and recovery of high-value compounds, Biomass Bioenergy. 150 (2021) 106141. https://doi.org/10.1016/j.biombioe.2021.106141.

[31] P. Brachi, V. Santes, E. Torres-Garcia, Pyrolytic degradation of spent coffee ground: A thermokinetic analysis through the dependence of activation energy on conversion and temperature, Fuel. 302 (2021) 120995. https://doi.org/10.1016/j.fuel.2021.120995.

[32] J. Fu, J. Liu, W. Xu, Z. Chen, F. Evrendilek, S. Sun, Torrefaction, temperature, and heating rate dependencies of pyrolysis of coffee grounds: Its performances, bio-oils, and emissions, Bioresour Technol. 345 (2022) 126346. https://doi.org/10.1016/j.biortech.2021.126346.

[33] S. Kelkar, C.M. Saffron, L. Chai, J. Bovee, T.R. Stuecken, M. Garedew, Z. Li, R.M. Kriegel, Pyrolysis of spent coffee grounds using a screw-conveyor reactor, Fuel Processing Technology. 137 (2015) 170–178. https://doi.org/10.1016/j.fuproc.2015.04.006.

[34] X. Li, V. Strezov, T. Kan, Energy recovery potential analysis of spent coffee grounds pyrolysis products, J Anal Appl Pyrolysis. 110 (2014) 79–87. https://doi.org/10.1016/j.jaap.2014.08.012.

[35] S.B. Kang, H.Y. Oh, J.J. Kim, K.S. Choi, Characteristics of spent coffee ground as a fuel and combustion test in a small boiler (6.5 kW), Renew Energy. 113 (2017) 1208–1214. https://doi.org/10.1016/j.renene.2017.06.092.

[36] M. Jeguirim, L. Limousy, E. Fossard, Characterization of coffee residues pellets and their performance in a residential combustor, Int J Green Energy. 13 (2016) 608–615. https://doi.org/10.1080/15435075.2014.888664.

[37] L. Limousy, M. Jeguirim, P. Dutournié, N. Kraiem, M. Lajili, R. Said, Gaseous products and particulate matter emissions of biomass residential boiler fired with spent coffee grounds pellets, Fuel. 107 (2013) 323–329. https://doi.org/10.1016/J.FUEL.2012.10.019.

[38] V. Bejenari, A. Marcu, A.M. Ipate, D. Rusu, N. Tudorachi, I. Anghel, I.E. Şofran, G. Lisa, Physicochemical characterization and energy recovery of spent coffee grounds, Journal of Materials Research and Technology. 15 (2021) 4437–4451. https://doi.org/10.1016/J.JMRT.2021.10.064.

[39] J. Chen, C. Xie, J. Liu, Y. He, W. Xie, X. Zhang, K. Chang, J. Kuo, J. Sun, L. Zheng, S. Sun, M. Buyukada, F. Evrendilek, Co-combustion of sewage sludge and coffee grounds under increased O2/CO2 atmospheres: Thermodynamic characteristics, kinetics and artificial neural network modeling, Bioresour Technol. 250 (2018) 230–238. https://doi.org/10.1016/J.BIORTECH.2017.11.031.

[40] J. Fu, X. Wu, J. Liu, F. Evrendilek, T. Chen, W. Xie, W. Xu, Y. He, Co-circularity of spent coffee grounds and polyethylene via co-pyrolysis: Characteristics, kinetics, and products, Fuel. 337 (2023) 127061. https://doi.org/10.1016/j.fuel.2022.127061.

[41] R. Nosek, M.M. Tun, D. Juchelkova, Energy Utilization of Spent Coffee Grounds in the Form of Pellets, Energies 2020, Vol. 13, Page 1235. 13 (2020) 1235. https://doi.org/10.3390/EN13051235.

[42] G. Allesina, S. Pedrazzi, F. Allegretti, P. Tartarini, Spent coffee grounds as heat source for coffee roasting plants: Experimental validation and case study, Appl Therm Eng. 126 (2017) 730–736. https://doi.org/10.1016/J.APPLTHERMALENG.2017.07.202.

[43] M. Jeguirim, L. Limousy, P. Dutournie, Pyrolysis kinetics and physicochemical properties of agropellets produced from spent ground coffee blended with conventional biomass, Chemical Engineering Research and Design. 92 (2014) 1876–1882. https://doi.org/10.1016/J.CHERD.2014.04.018.

[44] C.T. Primaz, Valorização de resíduos agroindustriais de café e algodão para produção de bio-óleo e biochar, Universidade Federal do Rio Grande do Sul, 2018. https://doi.org/http://hdl.handle.net/10183/190188.

[45] S. Yaman, Pyrolysis of biomass to produce fuels and chemical feedstocks, Energy Convers Manag. 45 (2004) 651–671. https://doi.org/10.1016/S0196-8904(03)00177-8.

[46] D. Mohan, C.U. Pittman, P.H. Steele, Pyrolysis of wood/biomass for bio-oil: A critical review, Energy and Fuels. 20 (2006) 848–889. https://doi.org/10.1021/ef0502397.

[47] C.T. Primaz, T. Schena, E. Lazzari, E.B. Caramão, R.A. Jacques, Influence of the temperature in the yield and composition of the bio-oil from the pyrolysis of spent coffee grounds: Characterization by comprehensive two dimensional gas chromatography, Fuel. 232 (2018) 572–580. https://doi.org/10.1016/J.FUEL.2018.05.097.

[48] J.P. Bok, H.S. Choi, Y.S. Choi, H.C. Park, S.J. Kim, Fast pyrolysis of coffee grounds: Characteristics of product yields and biocrude oil quality, Energy. 47 (2012) 17–24. https://doi.org/10.1016/j.energy.2012.06.003.

[49] W.T. Tsai, S.C. Liu, C.H. Hsieh, Preparation and fuel properties of biochars from the pyrolysis of exhausted coffee residue, J Anal Appl Pyrolysis. 93 (2012) 63–67. https://doi.org/10.1016/j.jaap.2011.09.010.

[50] S. Pinzi, C. Buratti, P. Bartocci, G. Marseglia, F. Fantozzi, M. Barbanera, A simplified method for kinetic modeling of coffee silver skin pyrolysis by coupling pseudo-components peaks deconvolution analysis and model free-isoconversional methods, Fuel. 278 (2020) 118260. https://doi.org/10.1016/j.fuel.2020.118260.

[51] C.L. Mendoza Martinez, J. Saari, Y. Melo, M. Cardoso, G.M. de Almeida, E. Vakkilainen, Evaluation of thermochemical routes for the valorization of solid coffee residues to produce biofuels: A Brazilian case, Renewable and Sustainable Energy Reviews. 137 (2021) 110585. https://doi.org/10.1016/j.rser.2020.110585.

[52] International Coffee Organization, The value of coffee. Sustainability, Inclusiveness, and Resilience of the Coffee Global Value Chain, 2020.

[53] F.J. Gómez-De La Cruz, F. Cruz-Peragón, P.J. Casanova-Peláez, J.M. Palomar-Carnicero, A vital stage in the large-scale production of biofuels from spent coffee grounds: The drying kinetics, Fuel Processing Technology. 130 (2015) 188–196. https://doi.org/10.1016/J.FUPROC.2014.10.012.

[54] M.M. Tun, H. Raclavská, D. Juchelková, J. Růžičková, M. Šafář, K. Štrbová, P. Gikas, Spent coffee ground as renewable energy source: Evaluation of the drying processes, J Environ Manage. 275 (2020) 111204. https://doi.org/10.1016/j.jenvman.2020.111204.

[55] T. Ciesielczuk, U. Karwaczynska, M. Sporek, The possibility of disposing of spent coffee ground with energy recycling, Journal of Ecological Engineering. 16 (2015) 133–138. https://doi.org/10.12911/22998993/59361.

[56] V. Dhyani, T. Bhaskar, A comprehensive review on the pyrolysis of lignocellulosic biomass, Renew Energy. 129 (2018) 695–716. https://doi.org/10.1016/J.RENENE.2017.04.035.

[57] J. Cai, D. Xu, Z. Dong, X. Yu, Y. Yang, S.W. Banks, A. V. Bridgwater, Processing thermogravimetric analysis data for isoconversional kinetic analysis of lignocellulosic biomass pyrolysis: Case study of corn stalk, Renewable and Sustainable Energy Reviews. 82 (2018) 2705–2715. https://doi.org/10.1016/J.RSER.2017.09.113.

[58] E. Torres-García, L.F. Ramírez-Verduzco, J. Aburto, Pyrolytic degradation of peanut shell: Activation energy dependence on the conversion, Waste Management. 106 (2020) 203–212. https://doi.org/10.1016/J.WASMAN.2020.03.021.

[59] S. Vyazovkin, A.K. Burnham, J.M. Criado, L.A. Pérez-Maqueda, C. Popescu, N. Sbirrazzuoli, ICTAC Kinetics Committee recommendations for performing kinetic computations on thermal analysis data, Thermochim Acta. 520 (2011) 1–19. https://doi.org/10.1016/J.TCA.2011.03.034.

[60] S. Vyazovkin, K. Chrissafis, M.L. Di Lorenzo, N. Koga, M. Pijolat, B. Roduit, N. Sbirrazzuoli, J.J. Suñol, ICTAC Kinetics Committee recommendations for collecting experimental thermal analysis data for kinetic computations, Thermochim Acta. 590 (2014) 1–23. https://doi.org/10.1016/J.TCA.2014.05.036.

[61] H.L. Friedman, Kinetics of thermal degradation of char-forming plastics from thermogravimetry. Application to a phenolic plastic, Journal of Polymer Science Part C: Polymer Symposia. 6 (2007) 183–195. https://doi.org/10.1002/polc.5070060121.

[62] T. Ozawa, A New Method of Analyzing Thermogravimetric Data, Bull Chem Soc Jpn. 38 (1965) 1881–1886. https://doi.org/10.1246/bcsj.38.1881.

[63] P.L. Vol, D. Method, F.O.R. The, D. Of, A. Energy, T.D. The, The land molluscs of the Krakatau Islands, Indonesia, Philosophical Transactions of the Royal Society of London. B, Biological Sciences. 322 (1988) 379–400. https://doi.org/10.1098/rstb.1988.0133.

[64] S. Vyazovkin, C.A. Wight, Model-free and model-fitting approaches to kinetic analysis of isothermal and nonisothermal data, Thermochim Acta. 340–341 (1999) 53–68. https://doi.org/10.1016/S0040-6031(99)00253-1.

[65] K. Miura, T. Maki, A simple method for estimating f(E) and k0(E) in the distributed activation energy model, Energy and Fuels. 12 (1998) 864–869. https://doi.org/10.1021/EF970212Q/ASSET/IMAGES/LARGE/EF970212QF00008.JPEG.

[66] J. Cai, Y. Chen, R. Liu, Isothermal kinetic predictions from nonisothermal data by using the iterative linear integral isoconversional method, Journal of the Energy Institute. 87 (2014) 183–187. https://doi.org/10.1016/J.JOEI.2014.03.019.

[67] G. Várhegyi, B. Bobály, E. Jakab, H. Chen, Thermogravimetric study of biomass pyrolysis kinetics. A distributed activation energy model with prediction tests, Energy and Fuels. 25 (2011) 24–32. https://doi.org/10.1021/EF101079R/SUPPL_FILE/EF101079R_SI_001.PDF.

[68] M. Hu, Z. Chen, S. Wang, D. Guo, C. Ma, Y. Zhou, J. Chen, M. Laghari, S. Fazal, B. Xiao, B. Zhang, S. Ma, Thermogravimetric kinetics of lignocellulosic biomass slow pyrolysis using distributed activation energy model, Fraser–Suzuki deconvolution, and iso-conversional method, Energy Convers Manag. 118 (2016) 1–11. https://doi.org/10.1016/J.ENCONMAN.2016.03.058.

[69] International Organization for Standardization, UNE-EN ISO 18122:2016 Solid biofuels. Determination of ash content., 2016.

[70] International Organization for Standardization, UNE-EN ISO 18123:2016 Solid biofuels. Determination of the content of volatile matter, 2016.

[71] International Organization for Standardization, UNE-EN ISO 18134-1:2016 Solid biofuels. Determination of moisture content - Oven dry method - Part 1: Total moisture - Reference method, 2016.

[72] M.V. Kok, E. Özgür, Thermal analysis and kinetics of biomass samples, Fuel Processing Technology. 106 (2013) 739–743. https://doi.org/10.1016/j.fuproc.2012.10.010.

[73] F. Rego, A.P. Soares Dias, M. Casquilho, F.C. Rosa, A. Rodrigues, Fast determination of lignocellulosic composition of poplar biomass by thermogravimetry, Biomass Bioenergy. 122 (2019) 375–380. https://doi.org/10.1016/j.biombioe.2019.01.037.

[74] F. Rego, A.P. Soares Dias, M. Casquilho, F.C. Rosa, A. Rodrigues, Fast determination of lignocellulosic composition of poplar biomass by thermogravimetry, Biomass Bioenergy. 122 (2019) 375–380. https://doi.org/10.1016/j.biombioe.2019.01.037.

[75] M. Hu, Z. Chen, S. Wang, D. Guo, C. Ma, Y. Zhou, J. Chen, M. Laghari, S. Fazal, B. Xiao, B. Zhang, S. Ma, Thermogravimetric kinetics of lignocellulosic biomass slow pyrolysis using distributed activation energy model, Fraser–Suzuki deconvolution, and iso-conversional method, Energy Convers Manag. 118 (2016) 1–11. https://doi.org/10.1016/J.ENCONMAN.2016.03.058.

[76] Z. Chen, M. Hu, X. Zhu, D. Guo, S. Liu, Z. Hu, B. Xiao, J. Wang, M. Laghari, Characteristics and kinetic study on pyrolysis of five lignocellulosic biomass via thermogravimetric analysis, Bioresour Technol. 192 (2015) 441–450. https://doi.org/10.1016/J.BIORTECH.2015.05.062.

[77] S. Naya, R. Cao, I.L. De Ullibarri, R. Artiaga, F. Barbadillo, A. García, Logistic mixture model versus Arrhenius for kinetic study of material degradation by dynamic thermogravimetric analysis, J Chemom. 20 (2006) 158–163. https://doi.org/10.1002/CEM.1023.

[78] Z. Cheng, W. Wu, P. Ji, X. Zhou, R. Liu, J. Cai, Applicability of Fraser–Suzuki function in kinetic analysis of DAEM processes and lignocellulosic biomass pyrolysis processes, J Therm Anal Calorim. 119 (2015) 1429–1438. https://doi.org/10.1007/s10973-014-4215-3.

[79] J.M. Cai, S.Y. Chen, R.H. Liu, Weibull mixture model for isoconversional kinetic analysis of biomass oxidative pyrolysis, Journal of the Energy Institute. 82 (2009) 238–241. https://doi.org/10.1179/014426009X12448189963559.

[80] A. Perejón, P.E. Sánchez-Jiménez, J.M. Criado, L.A. Pérez-Maqueda, Kinetic analysis of complex solid-state reactions. A new deconvolution procedure, Journal of Physical Chemistry B. 115 (2011) 1780–1791. https://doi.org/10.1021/JP110895Z/ASSET/IMAGES/LARGE/JP-2010-10895Z_0009.JPEG.

[81] S.I. Mussatto, E.M.S. Machado, S. Martins, J.A. Teixeira, Production, Composition, and Application of Coffee and Its Industrial Residues, Food Bioproc Tech. 4 (2011) 661–672. https://doi.org/10.1007/s11947-011-0565-z.

[82] B. Janissen, T. Huynh, Chemical composition and value-adding applications of coffee industry by-products: A review, Resour Conserv Recycl. 128 (2018) 110–117. https://doi.org/10.1016/j.resconrec.2017.10.001.

[83] H.L. Friedman, Kinetics of thermal degradation of char-forming plastics from thermogravimetry. Application to a phenolic plastic, Journal of Polymer Science Part C: Polymer Symposia. 6 (2007) 183–195. https://doi.org/10.1002/polc.5070060121.

[84] J.M. Criado, J. Málek, A. Ortega, Applicability of the master plots in kinetic analysis of non-isothermal data, Thermochim Acta. 147 (1989) 377–385. https://doi.org/10.1016/0040-6031(89)85192-5.

[85] L.A. Pérez-Maqueda, J.M. Criado, Accuracy of Senum and Yang's approximations to the Arrhenius integral, J Therm Anal Calorim. 60 (2000) 909–915. https://doi.org/10.1023/A:1010115926340.

[86] A. Khawan, D.R. Flangan, A. Khawam, D.R. Flanagan, Solid-state kinetic models: Basics and mathematical fundamentals, Journal of Physical Chemistry B. 110 (2006) 17315–17328. https://doi.org/10.1021/jp062746a.

[87] L.A. Pérez-Maqueda, J.M. Criado, F.J. Gotor, J. Málek, Advantages of combined kinetic analysis of experimental data obtained under any heating profile, Journal of Physical Chemistry A. 106 (2002) 2862–2868. https://doi.org/10.1021/jp012246b.

[88] A.W. Coats, J.P. Redfern, Kinetic Parameters from Thermogravimetric Data, Nature. 201 (1964) 68–69. https://doi.org/10.1038/201068a0.

[89] T.M. Mata, A.A. Martins, N.S. Caetano, Bio-refinery approach for spent coffee grounds valorization, Bioresour Technol. 247 (2018) 1077–1084. https://doi.org/10.1016/j.biortech.2017.09.106.

[90] C. Moliner, B. Bosio, E. Arato, A. Ribes, Thermal and thermo-oxidative characterisation of rice straw for its use in energy valorisation processes, Fuel. 180 (2016) 71–79. https://doi.org/10.1016/j.fuel.2016.04.021.

[91] C. Moliner, B. Bosio, E. Arato, A. Ribes-Greus, Comparative study for the energy valorisation of rice straw, 37 (2014) 241–246. https://doi.org/10.3303/CET1437041.

[92] H. Yang, R. Yan, H. Chen, D.H. Lee, C. Zheng, Characteristics of hemicellulose, cellulose and lignin pyrolysis, Fuel. 86 (2007) 1781–1788. https://doi.org/10.1016/J.FUEL.2006.12.013.

[93] D.K. Shen, S. Gu, K.H. Luo, A. V. Bridgwater, M.X. Fang, Kinetic study on thermal decomposition of woods in oxidative environment, Fuel. 88 (2009) 1024–1030. https://doi.org/10.1016/j.fuel.2008.10.034.

[94] H. Teng, Y.C. Wei, Thermogravimetric Studies on the Kinetics of Rice Hull Pyrolysis and the Influence of Water Treatment, Ind Eng Chem Res. 37 (1998) 3806–3811. https://doi.org/10.1021/IE980207P.

[95] C. Gomez, E. Velo, F. Barontini, V. Cozzani, Influence of Secondary Reactions on the Heat of Pyrolysis of Biomass, Ind Eng Chem Res. 48 (2009) 10222–10233. https://doi.org/10.1021/IE9007985.

[96] A. Iqbal, S.L. Badshah, J.L.F. Alves, J.C.G. da Silva, M. Di Domenico, An insight into the thermokinetics of the pyrolysis of invasive grass Sorghum halepense towards its bioenergy potential, Biomass Convers Biorefin. 1 (2022) 1–14. https://doi.org/10.1007/s13399-022-02697-6.

[97] B. Castells, I. Amez, N. Manic, D. Stojiljkovic, L. Medic, J. Garcia-Torrent, Kinetic study of different biomass pyrolysis and oxygen-enriched combustion, Thermal Science. 26 (2022) 4131–4145. https://doi.org/10.2298/TSCI2205131C.

[98] M. Carrier, L. Auret, A. Bridgwater, J.H. Knoetze, Using Apparent Activation Energy as a Reactivity Criterion for Biomass Pyrolysis, Energy & Fuels. 30 (2016) 7834–7841. https://doi.org/10.1021/acs.energyfuels.6b00794.

[99] R. Qi, A. Xiang, M. Wang, E. Jiang, Z. Li, H. Xiao, X. Tan, Combustion characteristics and kinetic analysis for pyrolysis char of torrefied pretreament from camellia shell, Biomass Convers Biorefin. 1 (2022) 1–12. https://doi.org/10.1007/s13399-022-02486-1.

[100] R. Moriana, Y. Zhang, P. Mischnick, J. Li, M. Ek, Thermal degradation behavior and kinetic analysis of spruce glucomannan and its methylated derivatives, Carbohydr Polym. 106 (2014) 60–70. https://doi.org/10.1016/j.carbpol.2014.01.086.

[101] M. Amutio, G. Lopez, R. Aguado, M. Artetxe, J. Bilbao, M. Olazar, Kinetic study of lignocellulosic biomass oxidative pyrolysis, Fuel. 95 (2012) 305–311. https://doi.org/10.1016/j.fuel.2011.10.008.

[102] M. Amutio, G. Lopez, R. Aguado, M. Artetxe, J. Bilbao, M. Olazar, Effect of vacuum on lignocellulosic biomass flash pyrolysis in a conical spouted bed reactor, Energy and Fuels. 25 (2011) 3950–3960. https://doi.org/10.1021/ef200712h.

[103] C. Şerbănescu, Kinetic analysis of cellulose pyrolysis: A short review, Chemical Papers. 68 (2014) 847–860. https://doi.org/10.2478/s11696-013-0529-z.

[104] G. Jiang, D.J. Nowakowski, A. V. Bridgwater, A systematic study of the kinetics of lignin pyrolysis, Thermochim Acta. 498 (2010) 61–66. https://doi.org/10.1016/j.tca.2009.10.003.

[105] T. Chen, L. Li, R. Zhao, J. Wu, Pyrolysis kinetic analysis of the three pseudocomponents of biomass–cellulose, hemicellulose and lignin: Sinusoidally modulated temperature method, J Therm Anal Calorim. 128 (2017) 1825–1832. https://doi.org/10.1007/s10973-016-6040-3.

[106] A. Galano, J. Aburto, J. Sadhukhan, E. Torres-García, A combined theoretical-experimental investigation on the mechanism of lignin pyrolysis: Role of heating rates and residence times, J Anal Appl Pyrolysis. 128 (2017) 208–216. https://doi.org/10.1016/J.JAAP.2017.10.009.

[107] T. Emiola-Sadiq, L. Zhang, A.K. Dalai, Thermal and Kinetic Studies on Biomass Degradation via Thermogravimetric Analysis: A Combination of Model-Fitting and Model-Free Approach, ACS Omega. 6 (2021) 22233–22247. https://doi.org/10.1021/ACSOMEGA.1C02937/ASSET/IMAGES/LARGE/AO1C02937_0008.JPEG.

[108] R. Moriana, Y. Zhang, P. Mischnick, J. Li, M. Ek, Thermal degradation behavior and kinetic analysis of spruce glucomannan and its methylated derivatives, Carbohydr Polym. 106 (2014) 60–70. https://doi.org/10.1016/j.carbpol.2014.01.086.

[109] Y. Ding, O.A. Ezekoye, S. Lu, C. Wang, R. Zhou, Comparative pyrolysis behaviors and reaction mechanisms of hardwood and softwood, Energy Convers Manag. 132 (2017) 102–109. https://doi.org/10.1016/J.ENCONMAN.2016.11.016.

[110] C. Moliner, K. Aguilar, B. Bosio, E. Arato, A. Ribes, Thermo-oxidative characterisation of the residues from persimmon harvest for its use in energy recovery processes, Fuel Processing Technology. 152 (2016) 421–429. https://doi.org/10.1016/j.fuproc.2016.07.008.

[111] A.L. Sullivan, R. Ball, Thermal decomposition and combustion chemistry of cellulosic biomass, Atmos Environ. 47 (2012) 133–141. https://doi.org/10.1016/j.atmosenv.2011.11.022.

[112] T. Chen, L. Li, R. Zhao, J. Wu, Pyrolysis kinetic analysis of the three pseudocomponents of biomass–cellulose, hemicellulose and lignin: Sinusoidally modulated temperature method, J Therm Anal Calorim. 128 (2017) 1825–1832. https://doi.org/10.1007/s10973-016-6040-3.

[113] J. Jauhiainen, J.A. Conesa, R. Font, I. Martín-Gullón, Kinetics of the pyrolysis and combustion of olive oil solid waste, J Anal Appl Pyrolysis. 72 (2004) 9–15. https://doi.org/10.1016/J.JAAP.2004.01.003.

[114] F. Shafizadeh, Pyrolysis and Combustion of Cellulosic Materials, Adv Carbohydr Chem. 23 (1968) 419–474. https://doi.org/10.1016/S0096-5332(08)60173-3.

[115] C.M. Santos, L.S. de Oliveira, E.P. Alves Rocha, A.S. Franca, Thermal conversion of defective coffee beans for energy purposes: Characterization and kinetic modeling, Renew Energy. 147 (2020) 1275–1291. https://doi.org/10.1016/j.renene.2019.09.052.

[116] O. Senneca, R. Chirone, P. Salatino, L. Nappi, Patterns and kinetics of pyrolysis of tobacco under inert and oxidative conditions, J Anal Appl Pyrolysis. 79 (2007) 227–233. https://doi.org/10.1016/J.JAAP.2006.12.011.

[117] X. Yang, D. Jiang, X. Cheng, C. Yuan, S. Wang, Z. He, S. Esakkimuthu, Adsorption properties of seaweed-based biochar with the greenhouse gases (CO2, CH4, N2O) through density functional theory (DFT), Biomass Bioenergy. 163 (2022) 106519. https://doi.org/10.1016/J.BIOMBIOE.2022.106519.

[118] Y.W. Low, K.F. Yee, A review on lignocellulosic biomass waste into biochar-derived catalyst: Current conversion techniques, sustainable applications and challenges, Biomass Bioenergy. 154 (2021) 106245. https://doi.org/10.1016/J.BIOMBIOE.2021.106245.

[119] K. Rasa, J. Heikkinen, M. Hannula, K. Arstila, S. Kulju, J. Hyväluoma, How and why does willow biochar increase a clay soil water retention capacity?, Biomass Bioenergy. 119 (2018) 346–353. https://doi.org/10.1016/J.BIOMBIOE.2018.10.004.

[120] A. Galano, J. Aburto, J. Sadhukhan, E. Torres-García, A combined theoretical-experimental investigation on the mechanism of lignin pyrolysis: Role of heating rates and residence times, J Anal Appl Pyrolysis. 128 (2017) 208–216. https://doi.org/10.1016/J.JAAP.2017.10.009.

[121] M.A. Lopez-Velazquez, V. Santes, J. Balmaseda, E. Torres-Garcia, Pyrolysis of orange waste: A thermo-kinetic study, J Anal Appl Pyrolysis. 99 (2013) 170–177. https://doi.org/10.1016/J.JAAP.2012.09.016.

[122] C.T. Chong, G.R. Mong, J.H. Ng, W.W.F. Chong, F.N. Ani, S.S. Lam, H.C. Ong, Pyrolysis characteristics and kinetic studies of horse manure using thermogravimetric analysis, Energy Convers Manag. 180 (2019) 1260–1267. https://doi.org/10.1016/J.ENCONMAN.2018.11.071.

[123] O. Gil-Castell, N. Mascia, C. Primaz, F. Vásqez-Garay, M.G.G. Baschetti, A. Ribes-Greus, Brewer's spent grains as biofuels in combustion-based energy recovery processes: Evaluation of thermo-oxidative decomposition, Fuel. 312 (2022) 122955. https://doi.org/10.1016/J.FUEL.2021.122955.